International Journal of Extreme Manufacturing

Nanofabrication of nanostructure lattices: from high-quality large patterns to precise hybrid units

Rui Ma, Xiaodan Zhang, Duncan Sutherland, Vladimir Bochenkov, Shikai Deng

View online: https://doi.org/10.1088/2631-7990/ad6838

Nanofabrication of nanostructure lattices: from high-quality large patterns to precise hybrid units

OPEN ACCESS
IOP Publishing | IMMT
International Journal of Extreme Manufacturing
Int. J. Extrem. Manuf. **6** (2024) 062004 (29pp)
https://doi.org/10.1088/2631-7990/ad6838

Topical Review

Nanofabrication of nanostructure lattices: from high-quality large patterns to precise hybrid units

Rui Ma[1,2], Xiaodan Zhang[1,2,3], Duncan Sutherland[4], Vladimir Bochenkov[5] and Shikai Deng[1,2,3,*]

[1] State Key Laboratory of Transducer Technology, Shanghai Institute of Microsystem and Information Technology, Chinese Academy of Sciences, Shanghai 200050, People's Republic of China
[2] 2020 X-Lab, Shanghai Institute of Microsystem and Information Technology, Chinese Academy of Sciences, Shanghai 200050, People's Republic of China
[3] School of Graduate Study, University of Chinese Academy of Sciences, Beijing 100049, People's Republic of China
[4] Interdiscplinary Nanoscience Center (iNANO), Aarhus University, 8000 Aarhus C, Denmark
[5] Department of Chemistry, Lomonosov Moscow State University, 119991 Moscow, Russia

E-mail: sdeng@mail.sim.ac.cn

Received 27 December 2023, revised 25 February 2024
Accepted for publication 27 July 2024
Published 13 August 2024

Abstract

Sub-wavelength nanostructure lattices provide versatile platforms for light control and the basis for various novel phenomena and applications in physics, material science, chemistry, biology, and energy. The thriving study of nanostructure lattices is building on the remarkable progress of nanofabrication techniques, especially for the possibility of fabricating larger-area patterns while achieving higher-quality lattices, complex shapes, and hybrid materials units. In this review, we present a comprehensive review of techniques for large-area fabrication of optical nanostructure arrays, encompassing direct writing, self-assembly, controllable deposition, and nanoimprint/print methods. Furthermore, a particular focus is made on the recent improvement of unit accuracy and diversity, leading to integrated and multifunctional structures for devices and applications.

Keywords: nanofabrication, nanostructure lattices, hybrid material structures, metasurfaces, large-area fabrication

1. Introduction

Optical nanostructure lattices are periodically arranged sub-wavelength units that can possess artificial optical properties such as negative refractive index and negative magnetic permeability [1–3]. The propagation features of light, including intensity, polarization, frequency, and phase, can be manipulated by designing the size, shape, orientation, or arrangement of units in these nanostructure lattices. The versatile light control through nanostructure lattices has significantly boosted developments of optical applications, such as optical sensing, enhancing photocatalysis, photodetection, lasing, etc [4–12]. Moreover, integration of nanostructures with other optical materials, such as phase-change materials, biomolecules, metal-organic frameworks

* Author to whom any correspondence should be addressed.

2631-7990/24/062004+29$33.00

(MOFs), two-dimensional (2D) materials, and perovskites, has dramatically enabled studies in light-matter interactions, showing great promise to the next generation of nanophotonic devices.

The bloom of the study on nanostructure lattices is building on the development of nanofabrication techniques, in which pattern generation, material deposition, etching, lift-off, and other pre- or post-treatment steps are usually included. Pattern generation can be summarized into two categories: top-down methods and bottom-up methods, according to the pattern directly given by artificially controlled beams or self-assembled/synthesized units, respectively. For top-down methods, direct writing techniques such as electron beam lithography (EBL), focus-ion beam lithography (FIB), and direct laser writing (DLW) can meet the requirement of high resolution and arbitrary patterning, allowing subtle tuning in nanostructures [13, 14]. Because of the compatibility with complementary metal oxide semiconductor (CMOS) fabrication, those writing methods are well-tested platforms for the validation of new designs and theories of nanostructure lattices. However, the low throughput and high cost are the main obstacles to the direct writing methods. From these direct writing approaches, further methods such as projection photolithography (including deep ultraviolet (DUV) and extreme ultraviolet (EUV) in the commercial CMOS fabrication) and interference lithography, are particularly developed to meet the requirement of large-area fabrication. For the bottom-up methods, self-assembly nanostructures allow the fabrication of large-scale lattices at low cost. The arrangement or bonding between self-assembled elements, such as colloidal nanoparticles, block copolymers, and DNA-origami, can form periodical nanostructures and patterns, thus being used for large-area fabrication as masks or selective sites. Another classification of bottom-up methods is controllable deposition, in which the growth process of the material can be artificially controlled by electromagnetic fields, masks, or chemical means. This type of one-step approach combining pattern generation and material deposition has received increasing attention in recent years due to its pattern flexibility, 3D printing capability, and low cost. Further, patterns generated either via direct writing or via self-assembled methods can be replicated and transferred to target substrates through imprinting or printing processes which can be operated at the macro level with nanometer resolutions.

The nanofabrication of nanostructure lattices is a balance between unit precision and pattern area while current methods are challenging to meet precision and efficiency simultaneously. Direct writing methods are more often used only for small-area prototype validation due to write speed limitations. Moreover, self-assembly methods are well-developed for nanostructure lattices but are still limited in the diversity of shapes and components of units. Efforts are made to propose sophisticated shapes beyond basic geometries, such as chiral, layered, core-shell, or mixed structures. Further, patterns fabricated through transfer methods are rigorously limited to the template written with lithography processes. There is great interest in using sophisticated process designs to obtain different nanostructures from a single template. Importantly, integration between nanostructure lattices and new material systems is emerging as promising platforms for novel photonic applications. Further possibilities for high performance, biocompatible, and dynamic lattices are also expected. The schematics of typical nanofabrication processes to generate diverse nanostructure lattices are summarized in figure 1.

Here, we present a comprehensive review of nanofabrication for nanostructure lattices. The main text is divided into two parts based on the two key aspects of the fabrication process: pattern generation and structural unit formation. Direct writing, self-assembly, controllable deposition, and nanoimprinting methods are introduced for lattice fabrication. Further, we highlight the fabrication and modification of structural units with complexity and hybrid structures. The summary and the prospects of lattice nanofabrication are provided at the end.

2. Top-down lithography

Top-down methods have a high degree of freedom in pattern design at the expense of fabrication times. Direct writing methods can write arbitrary 2D nanopatterns, but the reliance on a pixel-by-pixel exposure process greatly limits the size of generated arrays. Recent research efforts have focused on how to expand the area of direct writing to bring an improved balance between speed and precision in fabrication processes.

2.1. Direct writing techniques

Various types of beams or probes, such as nano-tips, electrons, focused ions, photons, and even atoms, are utilized for direct writing processes [15], while the target write layer could be a sensitive resist or planar thin films. Most writing lithography involves the utilization of beams to modify the local solubility of resist, enabling the formation of patterns that can serve as masks for subsequent etching or deposition processes [16, 17]. Moreover, by directly ablating, etching, or milling the material, or using the beams as a guidance of deposition, nanostructure lattices can be fabricated in a single step without the need for a photoresist. Direct writing techniques are mostly limited to 2D patterns with the same height, while 3D patterns have also been demonstrated. Direct writing methods are mask-free but low-throughput, that are usually employed to prepare micrometer-scale devices for proof of concepts. Fundamentals of direct writing have been extensively reviewed in previous works [14, 18–22]. In this section, we will provide a summary of the key concepts and features of these methods. The schematics of direct writing methods are shown in figures 2(a) and (b).

2.1.1. Electron beam lithography. Electron beam lithography (EBL) employs focused electron beams to generate patterns by changing the local solubility of the photoresist to the developer. EBL is widely used because of its nanometer-scale spatial resolution, relatively fast exposure, less damage to the substrate, and the ability to produce arbitrary patterns (figure 2(c)) or 3D structure (figure 2(d)). Compared to UV light, the electron beam can exhibit higher resolution due to its

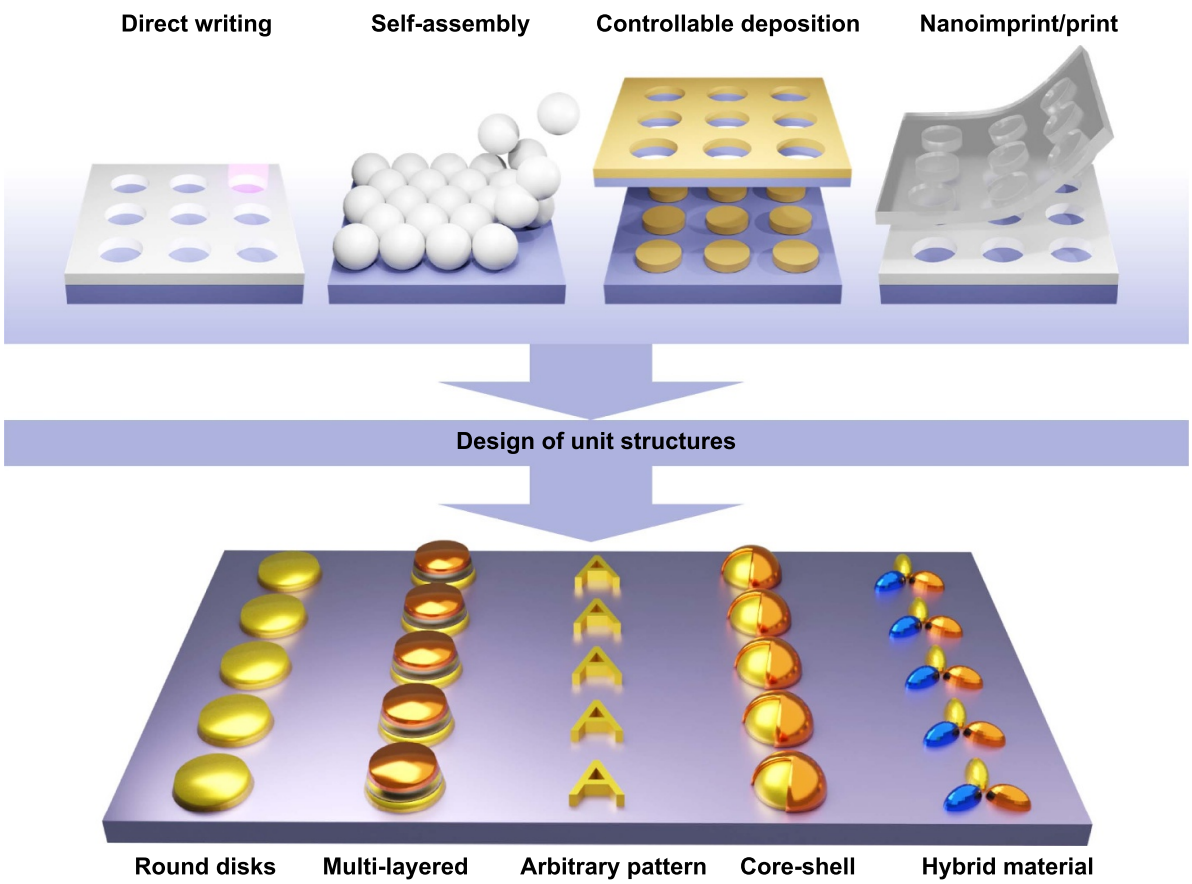

Figure 1. The overview of nanofabrication techniques for nanostructure lattices. Direct writing lithography and self-assembly, and pattern transfer methods for lattices fabrication. Nanostructural fabrication toward accuracy improvement, well-defined shapes, and hybrid structures. Diverse shapes and compositions of units are shown in the bottom schematic, including the round disk, multi-layered structure, arbitrary geometry, core-shell structure, and multi-material unit from left to right.

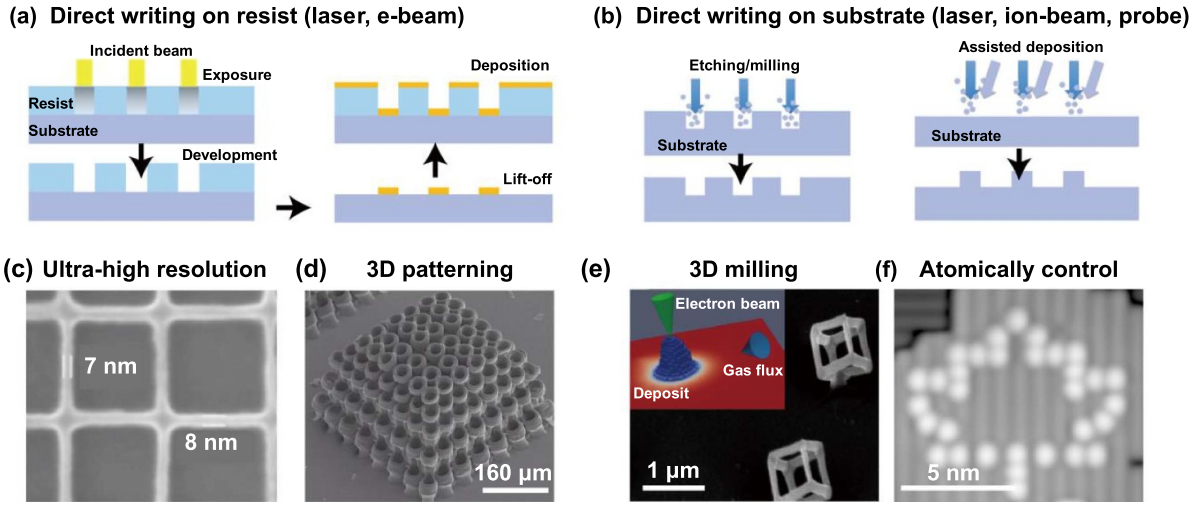

Figure 2. Direct writing methods for metasurfaces and nanostructures. (a) Schematic of typical direct writing methods applied on the resist. Patterns on the resist can be redirected onto the substrate by subsequent etching and deposition. (b) Schematic of typical direct writing methods applied on the substrate by direct etching/milling or assisted deposition. (c) A grid formed in ZnO with sub-10 nm resolution achieved by EBL. Reprinted from [23], Copyright © 2018 Elsevier Inc. All rights reserved. (d) 3D scaffold fabricated by two-photon polymerization writing. Reprinted from [24], Copyright © 2010 Acta Materialia Inc. Published by Elsevier Ltd. All rights reserved. (e) SEM image of nano-cubes fabricated by focused electron beam-induced deposition. The stem diameter (cylindrical), stem length, edge diameter (roughly elliptical), and edge length are 119 nm, 90 nm, 94/75 nm and 340 nm, respectively. The process of assisted deposition is attached in the inset. Reproduced from [25]. CC BY 4.0. (f) Scanning tunneling microscope image of the fabricated atomic pattern through hydrogen lithography. Reproduced from [26]. CC BY 4.0.

smaller wavelength. The injected electrons scatter and nonlinear processes in the resist are the main causes that prevent the pattern resolution from reaching its theoretical limit (∼1 nm). A common EBL system with a single beam has a writing speed range of 0.000 1–1.0 $cm^2 \cdot s^{-1}$ [27, 28]. For large-area nanostructure lattices with relatively low-resolution needs, fast exposure can be attained by increasing the current of exposure and using resist with high electron sensitivity, but still far from high-throughput requirement in mass production.

2.1.2. Focused-ion beam lithography. The focused-ion beam (FIB) method uses a beam of focused ions such as Ga and He ions to generate nanostructures and patterns. Ga is the most used ion beam source, while He ions have been developed with higher resolution, lower secondary electrons yield, and longer focus depth [29–31]. Due to the high accuracy and the ability to operate on the materials directly, FIB can be used as a tool for not only pattern generation but also pattern adjustment in a nanoscale area. The relationship between ion energy and the etching ability of common semiconductors has been summarized in a previous work [18]. Further, FIB can direct print 3D nanostructure with the feature size down to the order of 100 nm by a laser-assisted approach or post-growth purification [32–34], as shown in figure 2(e). In addition, the emitted ions can apply stress to the fabricated nanostructures, leading to a directional bending or folding in the nanoscale [35, 36].

2.1.3. Scanning probe lithography. The scanning probe lithography (SPL) (or dip-pen nanolithography, DPN) utilizes a micro-probe (Si with metal coatings [20, 37] or carbon nanotubes [38], etc) to scratch out the pattern in resist/material or guide the alignment of nanoparticles by heating and evaporation. Most SPL operates with probes shared from atomic force microscopy (AFM), scanning tunneling microscopy (STM), or near-field scanning optical microscopy (NSOM) [39–45]. The extreme resolution of SPL is relatively high compared with other writing methods, for example, hydrogen lithography, the removal of hydrogen atoms (depassivation) on hydrogen-passivated silicon surfaces based on STM with sharpened polycrystalline tungsten wire, can even reach atomic levels (figure 2(f)) [26, 37, 46, 47]. However, the aspect ratio of patterns is low because only shallow scratches can be achieved [48]. SPLs using mechanical stress of the probe can write at the speed of micrometer per second, while the thermal effect from tip heating can significantly increase the writing speed to the millimeter level, as called thermal scanning probe lithography (tSPL). However, the writing speed is limited to the fabrication of large-area lattices by the thermal reaction kinetics of materials and the mechanical movement speed of the probe.

2.1.4. Laser lithography. Direct laser writing (DLW) involves the utilization of lasers to modify the local solubility of the photoresist. Further, the laser fluence can ablate the substrate directly, be controlled to affect crystallization or ablation with different thresholds or facilitate controlled dewetting leading to the formation of nanoparticles [49–52]. With the development of laser technology, light sources with different characteristics offer a wide range of possibilities to enhance laser direct writing, such as improving ablation quality by means of femtosecond lasers through reduced exposure time, or achieving 3D printing by means of a two-photon polymerization lithography (TPL) [53–56]. Because the polymerization induced by two-photon absorption is a nonlinear absorption and in-volume process rather than a surface effect, a highly focused laser spatial point instead of a beam can be created for 3D writing with high resolution.

2.2. Large-area direct writing

Optimization of parameters can balance yield and precision within a certain range, however, direct writing sequentially at the micro-/nanometer scales falls short of meeting the requirement of the centimeter or even wafer scales in practical fabrication. To improve the writing efficiency, incorporating additional parallel beam sources or probes [57–59] and using high power ultra-fast lasers with a high precision displacement stage are intuitive and technically possible. On the other hand, the use of CMOS-compatible projection lithography is also a method for large-scale exposures, but a mask fabricated through direct writing methods is needed. Furthermore, optical device design gives great freedom in spatial beam manipulation, and one is thus able to achieve optical beam splitting and even independent control by means of interference, surface plasmon polaritons (SPP) excitation, and so on. High-throughput techniques for large-area patterning such as interference lithography and plasmonic lithography are developed. The comparison of different direct writing techniques and their large-area modification methods is summarized in table 1.

2.2.1. Writing with multiple beams or probes. By increasing the number of parallel beams or probes, it is an intuitive way to increase the speed of direct writing, especially for nano-array structures with periodically repeating units (figure 3(a)). This route was considered a solution for maskless lithography and is commonly used to increase the writing speed with electron beams and scanning probes. Parallel electron beam direct writing with around 1 000 beams was achieved in about 20 years ago [60, 61], however, the development of multi-electron beam direct writing is slow. In addition to industry inertia, the main reason is that its speed increase is still difficult to bring products from the micro-size to the macro large area. Further, multi probes scanning lithography attracts more attention in the past decades, and centimeter areas can be achieved with submicron resolution (figures 3(b) and (c)). Efforts are specially made to look for more durable probes, or a more homogeneous method of applying pressure [62–65].

2.2.2. Projection photolithography. Projection photolithography can simultaneously employ multiple writing beams by beam splitting through a mask rather than adding sources. This approach involves transferring patterns from a reusable mask created through direct writing methods to the photoresist

Table 1. The comparison among the techniques of direct writing techniques.

	Name	Beam	Resolution	Advantages	Challenges
Direct writing	DLW	Photons	∼100 nm	High tunability and moderate throughput	Diffraction limits resolution
	EBL	Electron	<10 nm	High resolution and high accuracy	Low throughput
	FIB	Focused ion	∼10 nm	High resolution and 3D printing	Slow writing speed, material resistance affects the accuracy
	SPL	Probe (through mechanical force, tunneling electrons, and thermal effect)	Atomic level (mechanical/tunneling); ∼10 nm (thermal)	High resolution, vacuum free, organic material compatible	Low throughput, poor aspect ratio
Large-area expansion of direct writing	Multiple beams or probes	Electron or probe	∼10 nm	Mask-free, high throughput with probes	Still low throughput with electrons
	Projection reprinting	Electron or photons	<10 nm	High throughput, resolution, and accuracy	Mask required, high equipment cost
	Ultrafast laser processing	Photons	>20 nm	High throughput and 3D printing	Limited materials
	Plasmonic lithography			High throughput, simple mask	Mostly periodic structures
	Interference lithography				

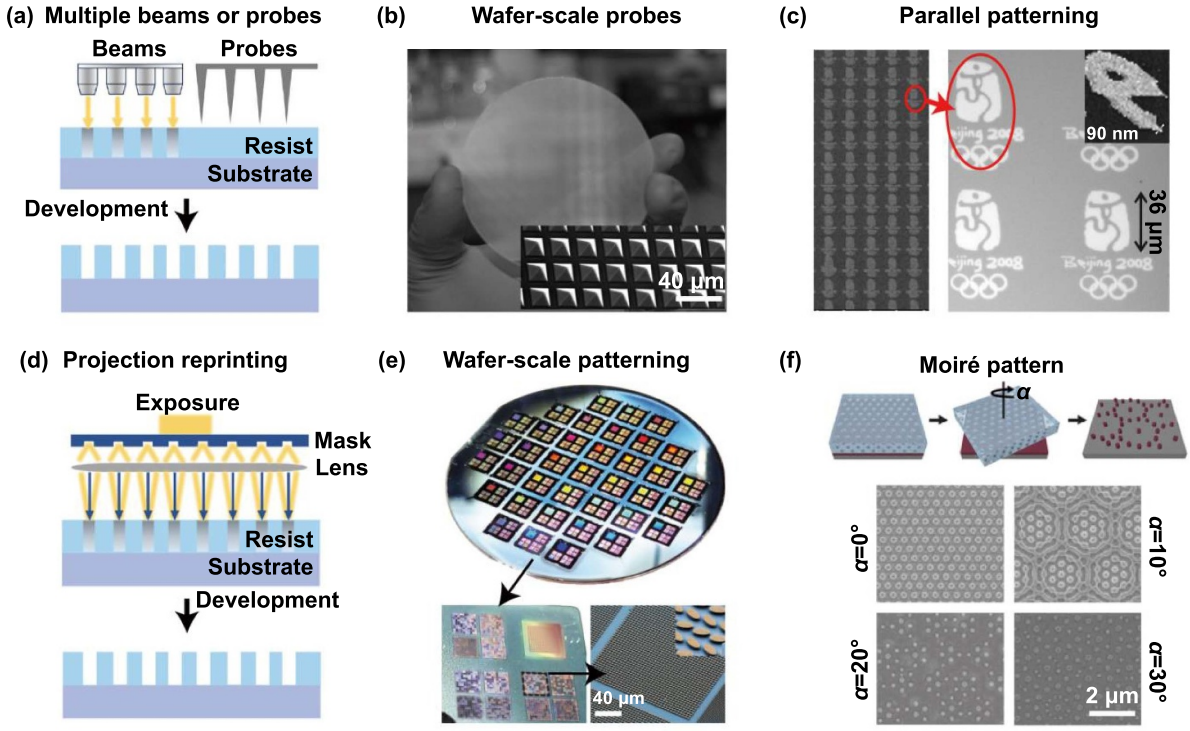

Figure 3. Writing with multiple beams or probes, and projection reprinting. (a) Schematic of lithography based on multiple beams or probes. (b) A photograph of an wafer with 11-million-pen array, and the inset shows the polymer tips with average radius (70 ± 10) nm. (c) Pattern written parallelly through multiprobes. The inset shows the 90 nm resolution captured from a letter 'e'. (b), (c) From [62]. Reprinted with permission from AAAS. (d) Schematic of projection reprinting. (e) Quasi-BIC metasurfaces fabricated by projection reprinting on a 4-inch wafer with 37 chips. One of the typical pixels in a chip has 100 different units with different structural designs. Reproduced with permission from [66]. © 2021 The Authors. Advanced Materials published by Wiley-VCH GmbH CC BY-NC-ND 4.0. (f) Schematic of Moiré nanolithography achieved by mask rotation. The different lattices with different rotated angles (0°−30°) are shown in the SEM images below. Reprinted with permission from [67]. Copyright (2012) American Chemical Society.

(figure 3(d)). To improve the resolution, light sources with short emission wavelengths, such as DUV at 193 nm and extreme ultraviolet (EUV) at 13.5 nm have been employed to mitigate subwavelength diffraction effects. The projection photolithography has been reviewed and widely utilized in commercial very-large-scale integrated circuits (VLSI) with over 3 nm accuracy [68–70]. As a representative top-down process, projection photolithography is a large-area and high-throughput method, but it still requires high costs and rigid substrates. As for the optical metasurfaces and nanostructure lattices, projection photolithography with DUV source has already enough for wafer-scale patterning (figure 3(e)). Fabrication of up-to 12-inch metasurfaces with sub-100 nm features has already been demonstrated [71–75]. The projection mask also offers an extra degree of freedom to tune the pattern. For example, a moiré pattern can be fabricated by multi-exposure with different orientations of the mask as shown in figure 3(f). In each exposure, the elastomeric mask was placed into direct contact with the resist to eliminate any translational effects. Up to 36-fold rotational symmetries were created, which led to expanded photonic band gaps and broadband wave transmittance. Such moiré patterns have the potential to be used in broadband or omnidirectional absorption region [67].

2.2.3. Ultrafast laser processing. Ultrafast laser processing (ULP) applies picosecond or femtosecond laser pulses to generate surface deformation by ablating processes. Fast exposure helps avoid damage from excessive thermal effects and excite focused nonlinear effects to improve resolution (figure 4(a)) [76, 77]. Specifically, the nonlinear multi-photon absorption in non-metallic materials shows threshold effects, providing a route to overcome the diffraction limit. Ultrafast laser exposure with highly precise and fast-moved stage offers ultra-high speed of writing, high throughput (4 mm^2 in timescales of units of minutes) fabrication of nanostructure lattices can be achieved [78] (figure 4(b)). Two-photon lithography (TPL) can generate three-dimensional or grey-scale pattern by using femtosecond laser to tune the chemical bonding between polymers or nanocrystals, leading to mask or direct structures [79–83]. The tunable phase by height change can shape the wavefront, boosting the development of diffractive optical elements to generate optical patterns in the far field [84, 85]. With the help of spatial light modulators, femtosecond regenerative amplifiers, and digital holographic techniques, parallel writing of TPL has also been realized [86, 87]. The writing speed has also been improved significantly, reaching 54 $mm^3 \cdot h^{-1}$ with 90 nm and 141 nm in lateral and axial directions in recent studies (figure 4(c)) [86].

2.2.4. Plasmonic lithography. Plasmonic lithography is another method to overcome the diffraction limit of light. A highly confined electromagnetic field in surface plasmon polaritons brings a large wave vector along the surface, leading to a much smaller plasmonic wavelength than incident light for exposure, and thus achieves resolution improvement (figure 4(d)) [92]. Moreover, the enhanced light intensity can be further distributed by structure patterning and polarization control with a large-area mask or prism, offering selectivity to the exposure and high-throughput [92, 93]. The pattern produced by surface plasmon polaritons depends on the near-field distribution on the nanostructures, therefore the structures on the mask act as probes or microlens. An effort has been able to achieve patterning one 12 inch wafer in minutes, which utilizes a plasmonic lens array containing 16 000 units, while the half-pitch resolution reaches as high as 22 nm (figure 4(e)) [88]. A recent study has fabricated sharp-edged nanodot patterns (with a 3.8 nm standard deviation of the side length, and ∼16.6 nm curvature radius for the 90° angle) through two-photon photochemical reactions of a photoresist, which is induced by plasmonic near-field light [94]. Another example shows that the excited polaritons can generate half-periodic ablations adjacent to the laser scanning path, leading to the formation of mismatched arrays within different depths [89] (figure 4(f)). This method offers a fast, maskless, and tunable fabrication of self-aligned nanostructures with no cleanroom condition required.

2.2.5. Interference lithography. Interference lithography is a process to generate periodic interference fringes through two or more coherent light sources for exposure, representing a rapid, mask-free, and large-area fabrication method (figure 4(g)). Two, three, or four-beam interference can create lines, hexagonal symmetry arrays, or rectangular symmetry arrays, respectively (figure 4(h)). Besides, the change of exposure dose can offer a degree of freedom in pattern modification (figure 4(i)). Interference lithography is suitable for the generation of arrays with simple unit geometry. Moreover, computer-aided design can be used to achieve more complex interference patterns in three dimensions for exposure through the design of independent beam interference or phase masks, known as holographic lithography [95–100]. In addition to the optoelectronic properties, the stress properties of the 3D lattices have recently received more attention, which advances the application of holographic lithography to large-area impact-resistant and piezoelectric materials [101–103]. As one of the candidates for wafer-scale fabrication, homogeneous distribution of exposure intensity along the entire substrate is required, while the applied interfered laser beams are usually with Gaussian distribution. A two-step process using a grayscale-patterned secondary exposure was developed to compensate for the linewidth difference in large area [104]. As low as 3.2 nm linewidth deviation all over the wafer-scale can be achieved in a highly uniform nano-grating or painting.

3. Self-assembled structures

The high precision and flexibility of direct writing technology to write arbitrary patterns is the reason for its wide use in the fabrication of nanostructure lattices. However, lattices with simple geometry such as square and hexagonal patterns are often used from collective electromagnetic oscillations, and arbitrary patterns are not required. Therefore, self-assembled particles with adjustable units can achieve fast lattice generation without need for costly lithography. Self-assembled

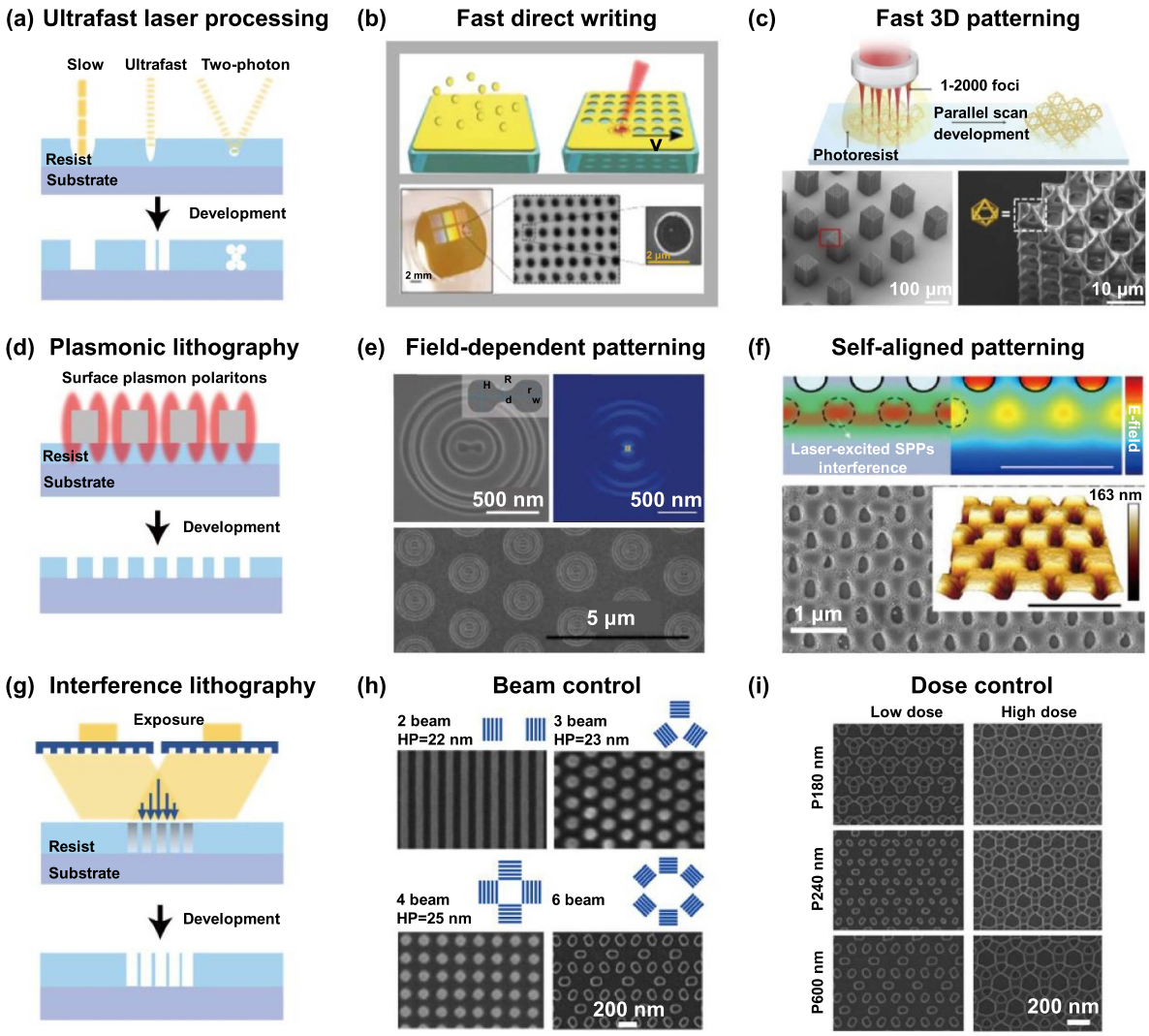

Figure 4. Fast writing by ULP, plasmonic lithography, and interference lithography. (a) Schematic of ultrafast laser processing. The short pulse of laser is used to avoid excessive ablation, and reduce exposure time. Nonlinear absorption excited by two pulses is used to perform 3D exposure. (b) The direct laser writing method is applied with ultrafast scanned lasers. The macroscopic view and SEM images of written nanoholes with a 3 μm period [78]. Reprinted with permission from [78]. Copyright (2012) American Chemical Society. (c) Printing process and results via multi-focus scanning. Complex 3D octahedral truss structures can be printed parallelly. Reproduced from [86]. CC BY 4.0. (d) Schematic of plasmonic lithography, where the excited local field is applied for exposure. (e) Dumbbell-shaped aperture arrays and its shape comparison with the excited local near-field. Reproduced with permission from [88]. Copyright © 2011, The Author(s) CC BY-NC-SA 3.0. (f) The SEM and AFM images show the 2D and 3D morphology of structures. The patterns correspond with the intensity distribution shown above, which is caused by the laser-excited surface plasmon polaritons. Reprinted with permission from [89]. Copyright (2022) American Chemical Society. (g) Schematic of interference lithography. Arrayed beams are generated by interference for exposure. (h) Schematics of different grating configurations in interference lithography. SEM images show the ability to expose different nanostructures with half-pitch (HP) and scale bar marked. Reprinted from [90], Copyright © 2015 Elsevier B.V. All rights reserved. (i) SEM images show the dose control in the interference lithography to pattern with different periods. Six beams with a 4π phase shift are applied to generate a Kagome lattice. Reprinted from [91], with the permission of AIP Publishing.

methods are bottom-up approaches that form patterns with molecules or nanoparticles [105, 106]. Specifically, self-assembled molecules can grow as bonding sites for units or forming patterns directly, while patterned nanoparticles can be used as a mask for further etching and deposition [107]. Nanostructure lattices fabricated through self-assembled methods find frequent applications in fields with high throughput requirements, including solar units, photocatalysts, and biosensing. Moreover, self-assembled molecules such as DNA origami allow patterning at the nanometer level, which remains challenging with direct writing methods. This section provides a summary of bottom-up assembly techniques for the preparation of nanostructure lattices (table 2).

3.1. Self-assembled nanoparticles

Colloidal nanospheres in solutions can experience various interactions to self-assemble on substrate surfaces, forming a robust mask for deposition, ablation, and etching processes (figure 5(a)) [108, 109]. By controlling the concentration of

Table 2. The comparison of different self-assembly techniques.

Methods	Source material	Accuracy	Advantages	Challenges
Colloidal lithography	Colloidal particles	<100 nm	Large-area pattern	Limited pattern geometry
Block copolymer	Block copolymer	~10 nm	Suitable for high density of units	Rough edge and high defect density, limited pattern and strict conditions
DNA-scaffolding	DNA origami	<10 nm	Small features, programmable DNA for arrangements, 3D patterning	Complicated process, environment sensitive

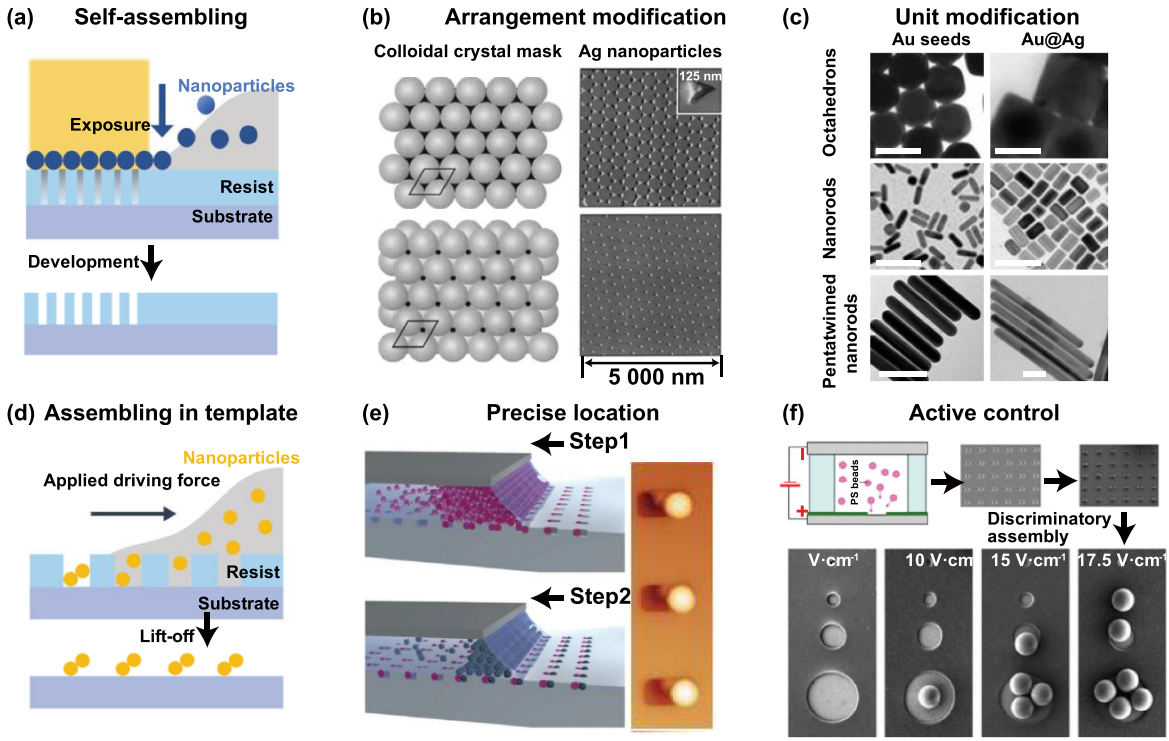

Figure 5. Assembled colloidal/nanosphere to form nanostructure lattices. (a) Schematic of assembly formation of nanopatterns without a pre-fabricated template. (b) Representative schematics and corresponding AFM images show the ability to change the generated patterns by changing the arrangement and stacking of nanoparticles. Reprinted with permission from [112]. Copyright © 2001, American Chemical Society. (c) SEM images show the morphological modification of assembled unit: different seeds and grown core-shell structures are fabricated (scale bar: 100 nm). Reprinted with permission from [113]. Copyright (2013) American Chemical Society. (d) Schematic of assembly formation of nanopatterns with pre-fabricated template. (e) Schematic shows the filling of nanoparticles in shape-matching recessed traps. The capillary force drags the receding contact line between the accumulation zone and the substrate, and the AFM image in the water showing PS-microgel dumbbells in the traps. Reproduced from [114]. CC BY 4.0. (f) SEM images show the location of selective particle assembly via electrophoretic deposition on the template. The schematic indicates the typical fabrication process including pre-patterned electrodes and electrophoretic deposition. Reprinted with permission from [115]. Copyright (2015) American Chemical Society.

nanospheres and deposition conditions, close-packed or loose monolayers of spheres can be achieved leading to periodic or non-periodic patterns on substrates (figures 5(b) and (c)). A common approach for creating well-ordered nanosphere masks involves their self-assembly at liquid interface followed by transfer to a solid substrate. Recent studies have shown that simple self-assembly can be achieved by air-drying nanoparticle solutions, and the choice of particle shapes enables the creation of asymmetric chiral nanostructures [110]. An oxygen plasma etching step can be then added to reduce the size of deposited polystyrene nanospheres while retaining their center-to-center distances [111].

Colloidal lithography has successfully been used to demonstrate the fabrication of both metal and dielectric nanostructures on hard or flexible substrates [116–118]. Additionally, the use of pre-patterned masks and self-assembled nucleation sites has become common practice to precisely position nanoparticles (figures 5(d) and (e)) [114, 119, 120]. This method can be considered a combination of particle self-assembly within a directly written template [121, 122], while the former provides organized particles and the latter provides accurate spatial placement in the nanoscale, respectively. Various driving forces, such as capillary force, dielectrophoresis, optical tweezers, magnetic fields, and electrophoretic deposition

(EPD), are employed to provide additional control over the assembly process (figure 5(f)) [115, 122–124]. Furthermore, simple dialing of the voltage during the EPD can be employed to verify the threshold for particle deposition. Colloidal lithography is widely adopted due to its cost-effectiveness, flexibility, and ease of implementation.

In addition to planar self-assembly nanoparticles, controlled self-assembly of multiple types of nanoparticles layer by layer can also be accomplished by setting up hierarchical microenvironments. Specifically, different single-crystalline metallic submicron polyhedral are synthesized via the polyol reduction route first, and close-packed dual structures within different layers are self-assembled through non-equilibrium distribution of different polyhedral within the droplet. Such distribution can be created by the dynamic particle transport arising from convective solvent flow during evaporation [125]. The orientation order can be further modulated during the interfacial self-assembly process through the orientational order established by identical facets, or induced model polymeric surfactants on the nanoparticle surfaces [126]. The superiority of this dual-structured supercrystal in terms of surface Raman scattering efficiency is then demonstrated, and potential applications are mentioned in mimicking natural dual crystals (such as the skin of a chameleon) or creating other artificial supercrystals.

3.2. Block copolymer lithography

Block copolymers are molecules composed of multiple distinct molecular segments that are connected covalently. These copolymers exhibit the ability to self-assemble into ordered structures at the molecular scale (figure 6(a)). Binary block copolymers are commonly used, including polystyrene-polyisoprene (PS-PI), polystyrene-polybutadiene (PS-PB), and polystyrene-polymethyl methacrylate (PS-PMMA) [127]. The process of organizing block copolymers into arrays typically involves spin-coating, thermal or solvent annealing, and degradation steps, and the modification of the interaction between the copolymer and substrate plays a critical role [128, 129]. To avoid the influence of substrate during the assembling, neutral interfaces are preferred [130–132]. Block copolymer lithography tuned by solvent and annealing has achieved a fabrication of nano-gratings with the highest resolution of $\sim$10 nm using PS-PDMS (figure 6(b)) [133–136]. By exploring new copolymer molecules, reducing their degree of polymerization, and increasing the degree of mutual incompatibility between blocks (i.e. Flory-Huggins factor), the feature size is expected to move towards 5 nm or even smaller. Moreover, efforts are made to adjust the pattern by changing annealing conditions or applying a template with patterned chemistry on the substrate (figure 6(c)) [128, 137, 138].

3.3. DNA-scaffolding

In the double-stranded helix structure of the deoxyribonucleic acid (DNA), nucleobases attached to each backbone, namely sugar and phosphate molecules, exhibit specific selectivity to pair with their counterparts on the opposite strand. By precisely engineering and scaffolding DNA through the programmed staple strand, such as through DNA origami, the nucleobase pairing ability can be harnessed for self-assembling nanostructure arbitrary patterning (figures 6(d) and (e)) [139, 141–145]. Chemically modified DNA sequences can be linked to inorganic nanoparticles in solution, leading to the formation of self-assembled nanostructures (figure 6(f)) [146–150]. This patterning technique enables the deposition of predefined binding sites, allowing for precise control of local hydrophilicity or charge to facilitate selective binding to the designated origami structures [151]. With a distance of 0.34 nm between each base pair and a strand diameter of 2 nm, this method offers promise for high-precision fabrication. Additionally, the oligonucleotide bonding elements exhibit dynamic interactions with visible light, as they undergo reversible structural changes in response to physical or chemical stimuli [140, 152].

4. Controllable deposition

Resist-based nanofabrication methods define patterns on the resist and enable material selection during the deposition. Controlled deposition refers to methods that directly control the material deposition or growth by some means to generate patterns in one step. This control can be physical, e.g. using a program-controlled electric field or a reusable physical mask, where the former can be simply seen as layer-by-layer printing at the microscopic level. Chemical control, on the other hand, is founded on controlling charge transfer or gas precipitation during the material synthesis to spontaneously generate periodic porous structures or templates. These methods are playing an increasingly important role in the preparation of large-scale lattice structures.

4.1. Gaseous ions deposition

Functional materials can be grown with periodicity at the nanometer level by applying appropriate physical and chemical guidance. For example, gaseous ions can be guided by fields to deposit at a specified location [153–155] (figure 7). Gas-phase cluster beams can deposit disordered nanoparticles directly to from atomic aggregations (figure 7(b)). Differential pumping-induced expansion is proposed to form a nanocluster beam as a source with the cluster of magnetron plasma gas, which is a potential cost-effective light extraction layer for commercialized LEDs [156]. Multilayers of horizontal electric fields and periodic circular perforations can guide the directional deposition of gaseous ions. Millimeter scale areas can be printed in tens of minutes [157, 158]. In addition to submicron accuracy, the electric field direct printing can reach high aspect ratio (figure 7(c)), 3D structures (figure 7(d)), and hybrid materials structures (figure 7(e)), which shows promise for diverse lattice preparation.

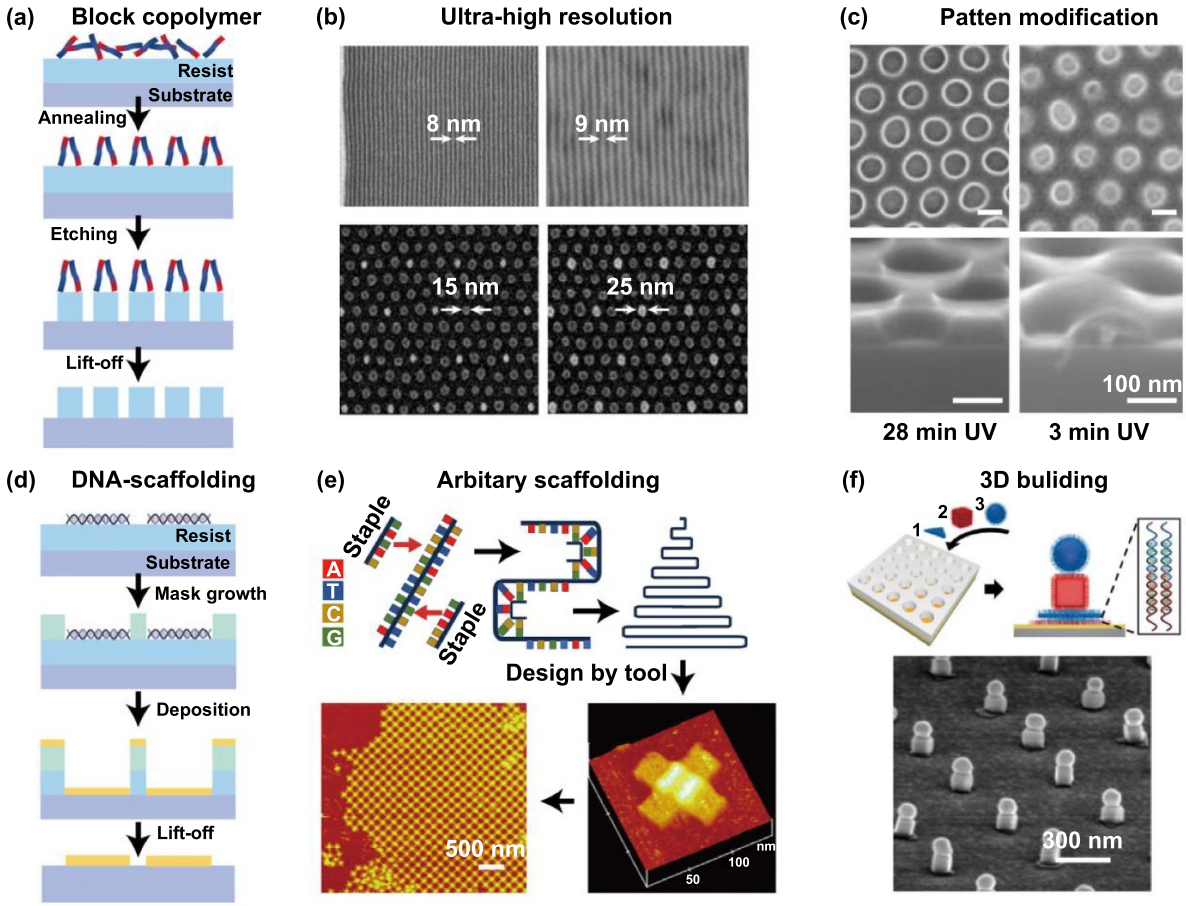

Figure 6. Assembled functional molecules to form periodic patterns. (a) Schematic of self -assembly methods based on block copolymer. (b) SEM images show the fabricated nano lines and particles, reaching the high resolution of 8 nm for lines and 15 nm for disks. From [133]. Reprinted with permission from AAAS. Reprinted with permission from [134]. Copyright (2010) American Chemical Society. (c) The plan-view and cross-sectional view of the hole patterns. UV exposure is applied to modify the pattern by time change. Reprinted with permission from [138]. Copyright (2022) American Chemical Society. (d) Schematic of self-assembly methods based on DNA-scaffolding. (e) The schematic of folding DNA helices by adding self-combined staple strand. AFM images of the single unit pattern and formed lattice by DNA folding are shown as well. [139] John Wiley & Sons. Copyright © 2011 WILEY-VCH Verlag GmbH & Co. KGaA, Weinheim. (f) Synthesis of oriented superlattices of two- and three-layer NP architectures. DNA-functionalized colloidal NPs are assembled by designing each layer of NPS to have a terminal DNA sequence complementary to that of the previous layer. From [140]. Reprinted with permission from AAAS.

4.2. Deposition through nanostencil

Nanostructure lattices can be fabricated through nanostencil without the need of conventional exposure-development process (figure 8(a)). The method relies on direct deposition of materials through a prepatterned reusable mask up to wafer scale [159]. Because of the absence of photoresist, the cost of a complete ventilation system is avoided and the contamination of substrate can be reduced. The main limitation of nanostencil is the conflict between the high difficulty of fabricating the stencil and its low durability. Specifically, the continuous material deposition alters the structural strength and patterned shape of the stencil itself. To solve this, a centimeter-scale reusable stencil processing using SiN stencils is proposed as an etch mask rather than a deposition mask (figure 8(b)) [160]. Moreover, the stencil is too thin and fragile due to the limitations imposed by the nanopatterning process. Existing studies have enabled the processing of PDMS soft stencils, thus avoiding the rigid fragmentation (figure 8(c)) [161, 162]. By synchronizing the substrate motion and material deposition, dynamic stencil lithography can be achieved. Stencil lithography has thus become a programmed pattern generation scheme similar to direct writing technology (figure 8(d)) [163]. In addition, inorganic stencil mask is usually more stable than photoresist, possessing the possibility to fit different deposition or growth requirements for metals or biological materials (figure 8(e)) [164, 165].

4.3. Electrochemical growth

Chemically controlled nanostructure fabrication mainly involves the reduction of metal ions, and the anodization-driven growth of metal oxide arrays. The inherent self-organization within the anode facilitates cost-effective, large-area production with high aspect ratios, making this technique readily applicable to a variety of transition metal oxides (figure 9(a)) [166, 167]. Aluminum oxide and titanium

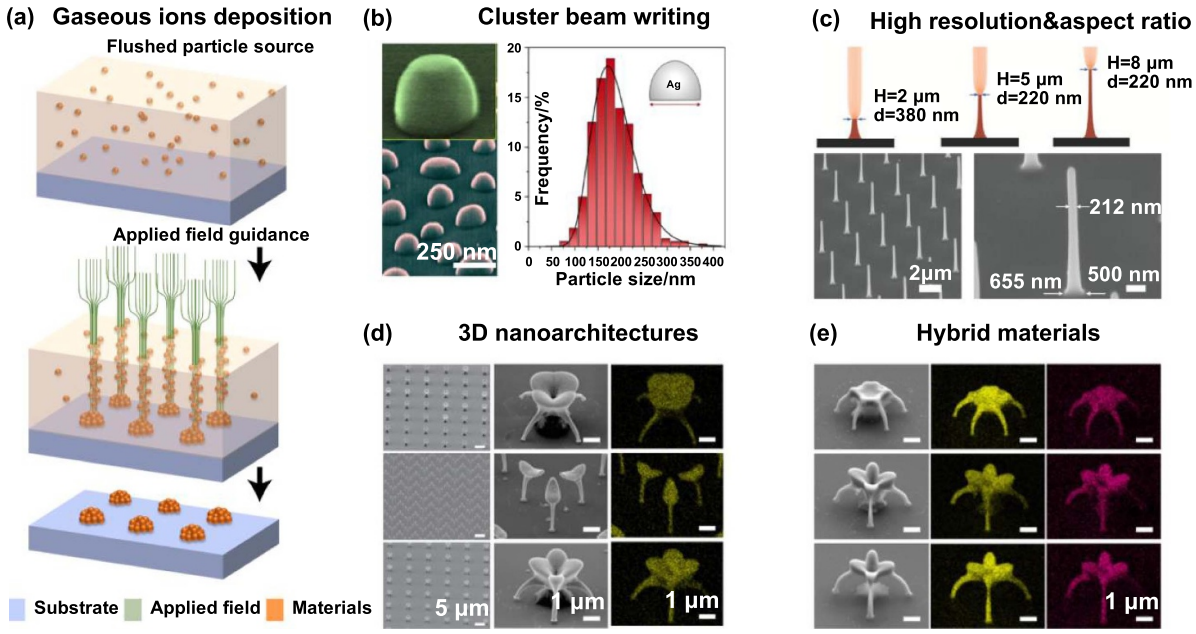

Figure 7. Gaseous ions deposition with applied patterned field control. (a) Schematic of gaseous ions deposition. Applied fields offer guidance to form patterned structures directly on substrate. (b) SEM images of the disordered Ag lattices fabricated by the gas-phase cluster beam deposition. The right panel shows the size distribution histogram of deposited nanoparticles (average diameter = 185 nm). Reproduced from [156]. CC BY 4.0. (c) Evolution of the pillar growth leads to lattices with nanostructures of 8 μm height and 220 nm diameter. [157] John Wiley & Sons. © 2023 Wiley-VCH GmbH. (d) SEM and EDS mappings show the 3D printing ability to the metal (Au) materials without resistance involved. (e) SEM and EDS mappings show the ability to print different materials (Au–Ag) into one nanostructure, which is achieved by flushing the chamber with different particle sources. (d), (e) Reproduced from [158]. CC BY 4.0.

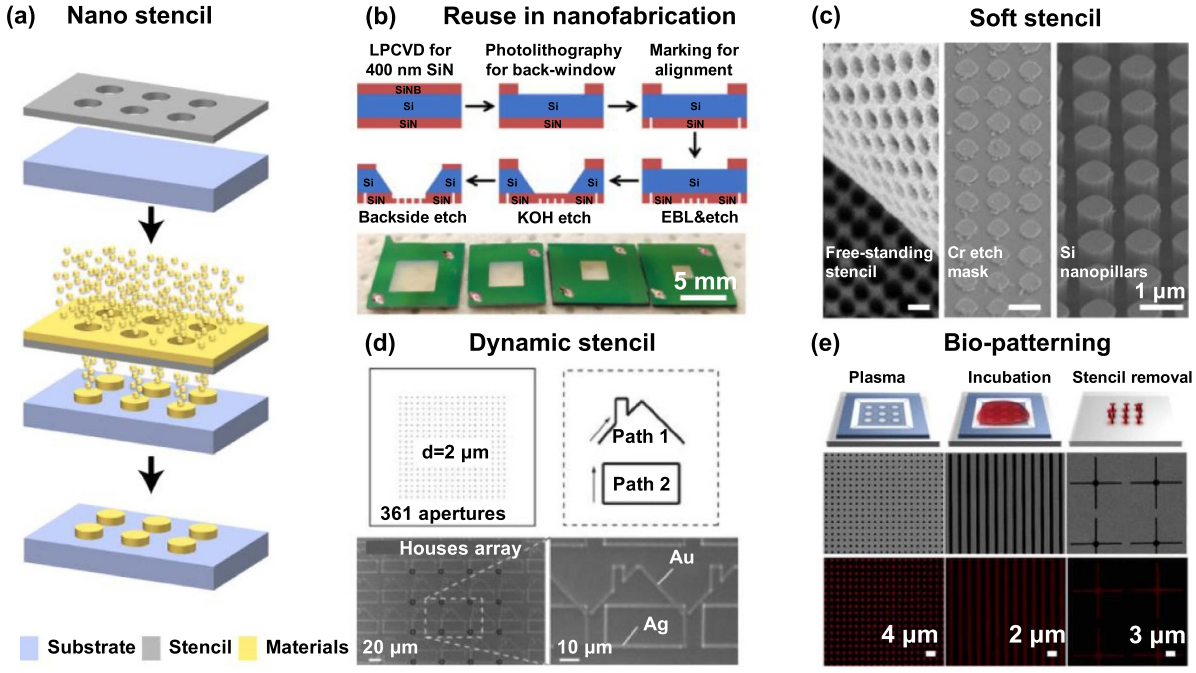

Figure 8. Nano stencil lithography. (a) Schematic of nano stencil lithography. (b) Schematic of the fabrication process for large-area SiN-based nano stencils, reaching millimeter level for fast patterning. Adapted with permission from [160] © The optical Society. (c) SEM images of the free-standing soft stencil. The fabricated structures are shown as Cr deposited structures before and after etching, forming mask arrays and Si nanopillars arrays, respectively. Reprinted from [161], with the permission of AIP Publishing. (d) Parallel fabrication of multi-materials surface structures (houses) made with dynamic stencil lithography. Reprinted from [163], with the permission of AIP Publishing. (e) Schematic diagrams of bio-patterning through nano stencil. The oxygen plasma process provides site-selection through the stencil by hydrophilic modification. Three different masks (SEM images) and corresponding fluorescence images of patterned antibodies are shown below. Reprinted with permission from [164]. Copyright (2012) American Chemical Society.

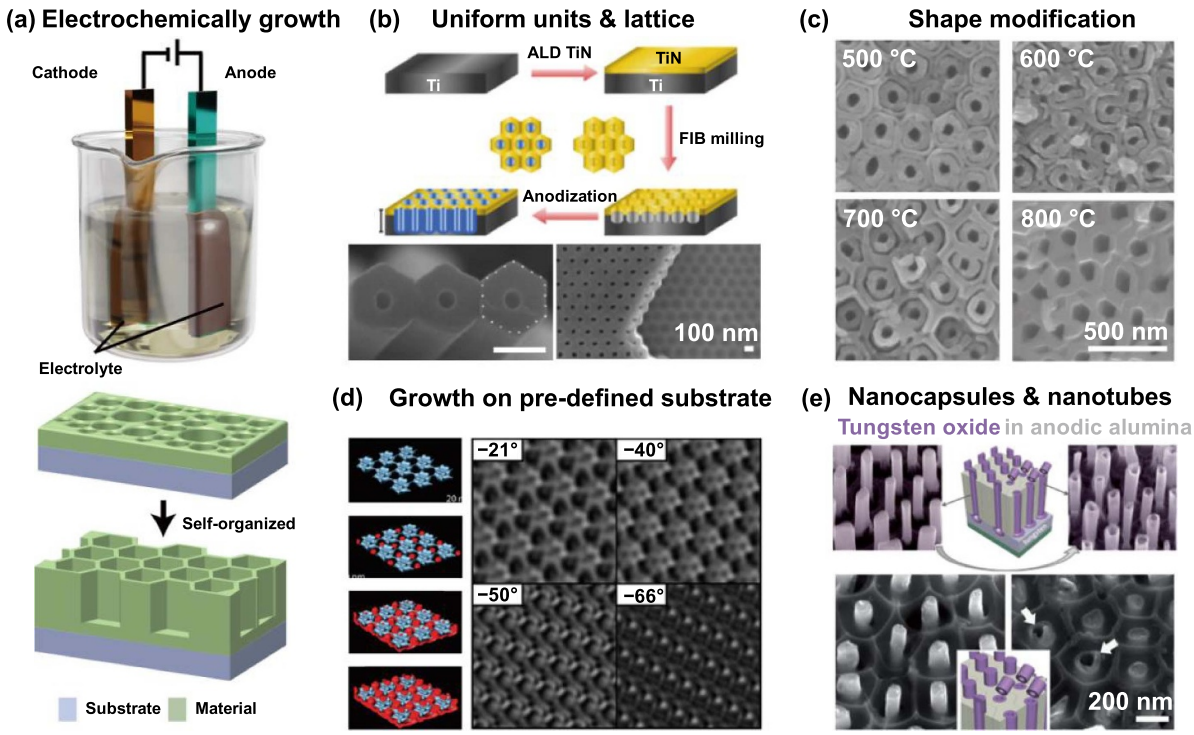

Figure 9. Electrochemically growth of nano lattices. (a) Schematic of typical anodization synthesis which leads to rapid, low-cost, and large-area fabrication. (b) Ideally hexagonally nanotubes can be further grown with a pre-texturing substrate. Reproduced with permission from [166]. © 2017 The Authors. Published by Wiley-VCH Verlag GmbH & Co. KGaA. CC BY-NC 4.0. (c) Sequence of SEM images showing the shape modification of TiO_2 nanotubes through annealing in different temperatures. [168] John Wiley & Sons. Copyright © 2008 WILEY-VCH Verlag GmbH & Co. KGaA, Weinheim. (d) The 3D architecture of cuprous oxide electrochemically deposited through the pores of the hexagonally packed intermediate surface-layer protein from Deinococcus radiodurans SARK. Right panel shows the representative TEM tilt series for electrodeposited cuprous oxide (dark) grown through the HPI-layer protein (light) along one of two orthogonal tilt axes. Reprinted with permission from [172]. Copyright (2008) American Chemical Society. (e) The pore-directed TO nanocapsules/nanorods arrays are selectively grown, which can be electrochemically top-opened in alumina nanopores and transformed to TO nanotubes. Reproduced from [175]. CC BY 4.0.

dioxide hole arrays are the most common cases of anodization growth, possessing distinct periodic submicron lattice structures which can be further homogenized and regularized (figure 9(b)). By adjusting the anodization parameters and subsequent thermal processes, the size, shape, degree of order, and crystalline phases of the metal oxides can be modified (figure 9(c)) [168–171]. In addition, electrochemical growth on the substrate with predefined lattices also allows further expansion of the morphology of the lattice units, such as three-dimensional structures [172] and in-plane polystructures [173] (figure 9(d)). The anodized lattice is usually with porous units, and if such a surface is used as a substrate for further material deposition or a second anodizing of a different material, more morphological array structures can also be obtained (figure 9(e)). Although some work has explored the use of anodization lattices as masters to make more classical lattices [173, 174], structures prepared by anodization methods are more often used only to make specialized materials in batteries or biomaterials. This is mainly because the structure and material are limited to a small number of choices.

5. Nanoimprint/print lithography

Structured molds can be embossed or printed for mass production of nanostructure arrays, known as nanoimprint and micro-contact printing. Nanoimprint lithography (NIL) involves molding and demolding processes to transfer nanoscale patterns from a topographically structured master. Both liquid [176, 177] and solid [178–182] states of matters have been covered by nano molding to generate patterns [183–185], such as polymers [186–190], metallic glasses [191–200], alloys [201–203] and metals [204–206]. Micro-contact printing is similar to conventional printing, using a PDMS material that has undergone surface single-molecule self-assembly in a thiol-based solvent as both ink and etch mask. These approaches enable the attainment of both high throughput and cost-efficient production once the initial master is fabricated. Although the masters are fixed once fabricated, structural adjustment is allowed through parameters control during the fabrication processes. According to the different embossing processes, nanoimprint and print methods can be classified

Table 3. The comparison of different imprint methods.

Imprint Method		Mold	Advantages	Challenges
Thermal NIL		Si, SiO_2, Si_3N_4, SiC	High versatility in materials and size	High temperature and pressure, hard master with low lifespan
UV-NIL		Quartz, SSQ, PDMS	High alignment accuracy (transparent master for observation), fast curing, and suitable for roll-to-toll processing	Transparent master or substrate must be required
Solvent-assisted methods	SANE	PDMS	Low-cost, vacuum free	Limited applicable materials
	Micro-contact printing		Less contact leads to better protection of the master	Low resolution

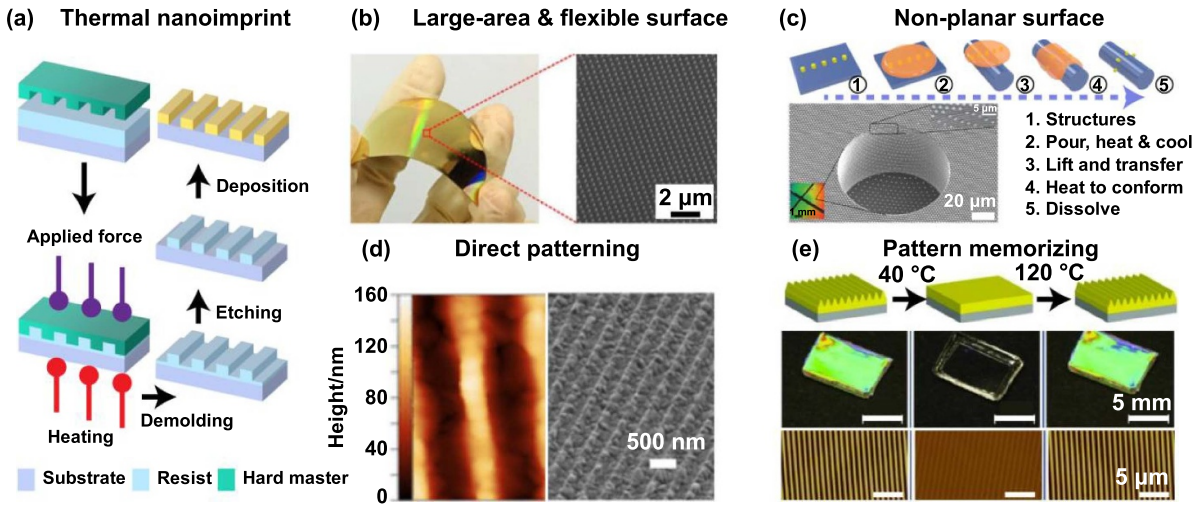

Figure 10. Pattern transfer through thermal nanoimprint. (a) Schematic of thermal nanoimprint. Applied force and heating are both necessary for tight contact between master and resist. (b) Photos and SEM images of large-area nanostructure lattices fabricated using Thermal NIL. Reprinted from [214], © 2019 Elsevier B.V. All rights reserved. (c) Process steps (from 1 to 5) and the transferred disk pattern onto a surface with 100 μm-diameter, 50 μm-deep holes. From [215]. Reprinted with permission from AAAS. (d) Direct nanoimprint onto perovskite films shown on AFM and SEM images. The average roughness of the gratings can reach as small as 4.4 nm. Reprinted with permission from [216]. Copyright (2023) American Chemical Society. (e) Schematic and corresponding pattern memory cycle in an acrylate-based polymers. The period and height of the gratings are 834 nm and 179 nm, respectively. [217] John Wiley & Sons. Copyright © 2011 WILEY-VCH Verlag GmbH & Co. KGaA, Weinheim.

into three categories: thermal embossing nanoimprint (thermal NIL), ultraviolet nanoimprint (UV NIL), and solvent-assisted methods (table 3). Nanoimprint methods can easily reach sub-20 nm resolution which is far below the diffraction limit of the typical photolithography [207–210].

5.1. Thermal nanoimprint/print lithography

Nanoimprinting was first proposed with the thermal embossing method in 1995 [186]. Thermal NIL typically includes a heating process to soften the coated thermoplastic photoresist (usually PMMA) on the substrate, allowing it to be pressed into a pre-patterned stencil by mechanical force. High pressure is maintained during the subsequent cooling process (figure 10(a)). Patterns are transferred onto the photoresist after the release of the master, while the residual photoresist can be removed by the reactive ion etching process. In addition, transferring patterned structures directly between substrates can also be achieved through similar routes, which can be referred to as thermal printing or thermal transfer technology [211–213].

Thermal nanoimprint is simple and highly compatible with existing materials and semiconductor fabrication [179]. A recent work suggests one of the cheapest resists under the thermal nanoimprint routes: regular table sugar (sucrose) [216]. The low thermal transition temperature of sucrose and solubility in water provides great convenience for molding, demolding and surface cleaning. Compared to other lithography routes, it can easily give the flexibility to process micro- and nanostructures directly on flexible (figure 10(b)), non-planar (figure 10(c)) or target materials (figure 10(d)) substrates [214–216, 218, 219]. Typical thermal embossing usually employs hard master to prevent the effects of thermal expansion and contraction, but hard master is more expensive

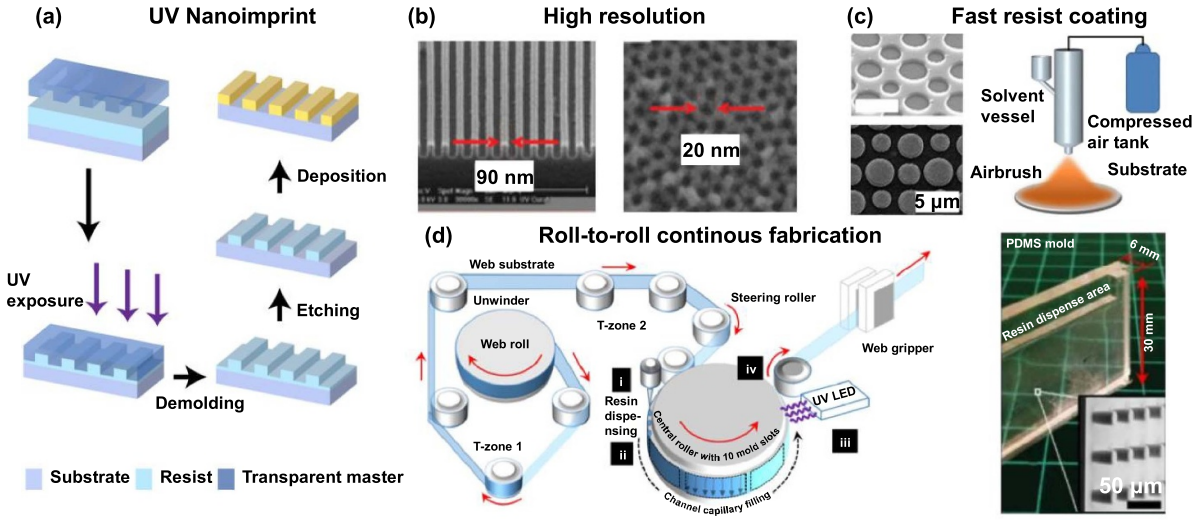

Figure 11. Pattern transfer through UV nanoimprint. (a) Schematic of UV nanoimprint. Ultraviolet exposure is applied instead of heating for the curing of resist. (b) Epoxysilsesquioxane (SSQ)-based resist with seconds of UV solidification time can reach as high as high as 90 nm and 20 nm resolution in grating and array structures [224]. Reprinted with permission from [224]. Copyright (2010) American Chemical Society. (c) By airbrushing instead of spin coating, the diluted polymer (SSQ) can be coated faster for continues nanoimprint. The master and printed structures are shown on the left [225]. Reproduced from [225]. CC BY 4.0. (d) Roll-to-roll (R2R) imprinting fabrication system with a high throughput of up to 3000 $mm^2 \cdot min^{-1}$ with fast UV embossing. The applied PDMS mold is shown on the right with the images of its micropillar arrays. Reprinted with permission from [226]. Copyright (2018) American Chemical Society.

to be prepared and the microstructures are more vulnerable. On the other hand, such deformation properties of soft master can be exploited in certain cases to achieve fast shape adjustment of pattern memory (figure 10(e)) [217, 220]. Such methods provide solutions for programmable scaling of embossing patterns from one single master.

5.2. UV nanoimprint lithography

The use of UV-sensitive resist instead of thermal resist in the embossing process effectively avoids damage to the master caused by heating and high pressurization, leading to an extended lifespan for the mold and reduced costs [221]. UV-NIL photoresists are typically low-viscosity and UV-sensitive liquid polymers, therefore the mold materials need to be transparent to UV light, such as quartz glass (hard mold) or PDMS (soft mold). After the mold is pressed into the photoresist, UV light is irradiated to polymerize and cure the photoresist into patterns (figure 11(A)) [222, 223].

Photocurable silsesquioxane (SSQ) resins can reach linewidth resolution below 100 nm (figure 11(b)), while possessing fast curing (seconds level), low shrinkage, no oxygen inhibition, no outgassing, high modulus, easy release, good coat-ability, and high etch resistance [224]. In addition to conventional spin coating, a new airbrushing method was developed for SSQ (figure 11(c)) [225]. The coated resin film thickness can be readily tunned by the controlling of polymer concentration in solvent and airbrushing time. The use of soft master, fast UV curing, and resist coating allow for continuously roll-to-roll embossing equipment designed with much higher efficiency than hot embossing (figure 11(d)). Multi-layered nanostructures can be obtained by multiple imprinting, i.e. by first imprinting a substrate with a pattern of micron-sized micropores (20 μm), and then imprinting a PDMS micropillar mold (550 nm in diameter) with this substrate to produce membranes with multi-scale micropores, which greatly simplifies the fabrication process of hierarchical porous membranes [226].

5.3. Solvent-assisted methods

Based on the hard master protection or the conformability of soft masters requirements, solvent-assisted methods are developed to reach more gentle embossing or micro-contact printing. In solvent-assisted nanoimprint embossing (SANE) technique, the mold is wetted with organic solvents before contacting the photoresist-coated substrate [227]. These organic solvents can dissolve (or swell) the photoresist film on the contact surface to create a local fluid containing both polymer and solvent to match the mold. The polymer cures gradually with the evaporation of the solvent while the mold remains in conformal contact with the substrate. In micro-contact printing, PDMS materials undergo surface single-molecule self-assembly in alkanethiol-based solvents and serve as printing inks and etching masks. The schematics of both methods are shown in figure 10(a). These methods reduce the cost of mastering and can be implemented with simple tools without the need for a lot of equipment such as heating and pressurization, irradiation, vacuum chamber, etc. However, readily achieved resolutions of nanostructures are lower than those of thermal and UV embossing.

SANE with its fast-embossing process and good protection of the substrate is used for the rapid preparation or tuning of some reconfigurable arrays. A single step for

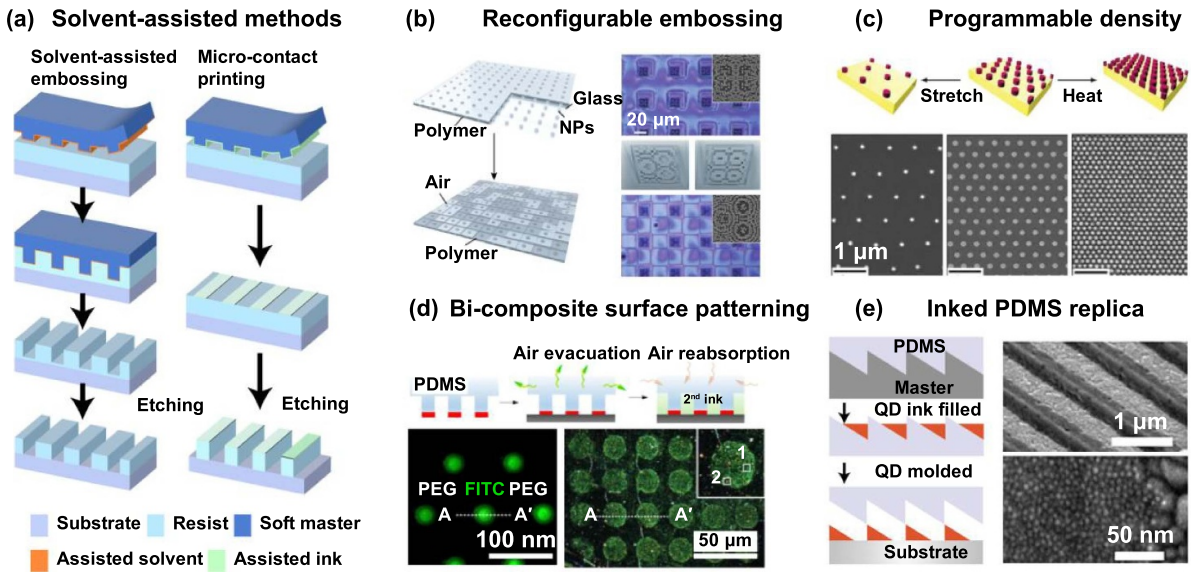

Figure 12. Pattern transfer through solvent-assisted methods. (a) Schematic of typical solvent-assisted methods, including SANE and micro-contact printing. Solvent is used as a dissolution coating embossed in cured resist, or an ink that acts as a mask for etching. (b) Reconfiguration schematic and results of metalenses with 4 or 3 focus points in one unit. Reprinted with permission from [228]. Copyright (2019) American Chemical Society. (c) Up to 100% spacing increment and 50% decrement of period can be achieved by stretching or heating within a SANE process. Simultaneously, the feature sizes as small as 45% can be controlled from swelling of patterned molds with different solvents. Reprinted with permission from [229]. Copyright (2019) American Chemical Society. (d) Schematic illustration of the two-steps micro-contact print. Two different inks are printed on the substrate leading to disks of FITC-BSA surrounded by PEG-silane (left). Further bonding steps can create Au nanoparticles arrays (right). Reproduced from [231]. CC BY 4.0. (e) Direct molding of ligand-capped CdSe quantum dots from PDMS replica stamps. The stamp was held at a low angle so as to facilitate smooth draining of the toluene during drying. Reprinted with permission from [232]. Copyright (2009) American Chemical Society.

erasing and writing the polymer was introduced with a tunable focusing metasurface (figure 12(b)). This work combines a three layered metasurface including PDMS metalens, polymer and nanoparticles arrays, where adjusting the PDMS master enables rapid reconfigurable switching of imaging focusing statuses [228]. Further, adjustment of strain, temperature and solution properties allows a full control of period and structural size of imprinted arrays without the need for new masters (figure 12(c)) [229, 230]. Varying the size of the patterned photoresist can be achieved using different degrees of dissolution of PDMS in various solvents. For example, using the same mold but using dimethylformamide ($S = 1.02$, S was defined as the swelling factor), isopropyl alcohol ($S = 1.09$), and dichloromethane ($S = 1.22$) as solvents resulted in a 22%, 33% and 44% reduction in the size of the patterned features, respectively. Moreover, the pitch remained almost unchanged (pitch changes <3 nm in some areas) while the pattern was intact [229].

Due to the limitations of the ink delivery process, micro-contact printing cannot achieve as high resolution as SANE for now, and the choice of ink also limits the application of micro-contact printing. However, since there is no embossing process, microcontact printing provides additional ideas for the design of structures and preparations. A recent work fabricated a bi-composite micropatterned surface through combining micro-contact printing and microfluidic vacuum-assisted degas-driven flow guided patterning (DFGP). Through the permeation of the second ink into the free cavity of the PDMS stamp under negative pressure created by the degassed PDMS, composite biomolecular arrays had been used to direct cell adhesion, polarization, or the assembly of metal particles (figure 12(d)) [231]. Compound quantum dot (QD) solutions can also be used as printing inks to fabricate QD arrays by single-step printing (figure 12(e)). In this work, low-angle stamps were designed to facilitate solution drainage during the drying process [232].

6. Control of unit structures

Pattern generation methods such as direct writing, self-assembly, controllable deposition, and nanoimprint, are well-developed and have been employed for the typical fabrication of nanostructure lattices. These methods are well established for fabricating nanolattices composed of basic geometries but still face limitations. For example, rigid substrates and specialized equipment required for large-scale writing, patterns generated by self-assembly techniques are limited by the self-assembled particles themselves, photolithography and nanoimprinting rely on expensive direct-writing techniques to create masks, controlled deposition is limited by the deposition properties of the particular material, etc. Recent studies focus on breaking the inherent limits of traditional techniques to achieve higher resolutions or novel unit features for unprecedented optical performances of nanostructure lattices. These explorations can be summarized into three categories: improving the resolution and aspect ratio of direct writing techniques, expanding the diversity of unit structures

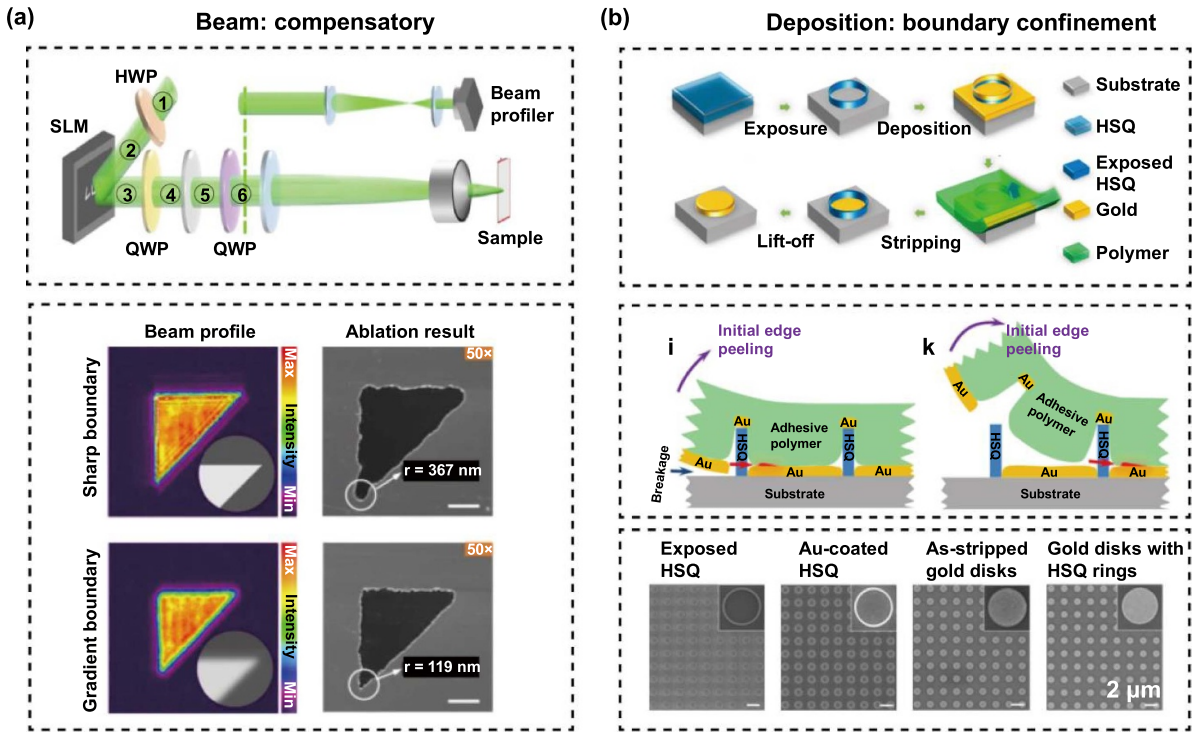

Figure 13. Improvement of fabrication accuracy through process optimization. (a) Upper panel: schematic of the lithography system with patterned pulse laser (QWP: quarter waveplate, HWP: half waveplate, SLM: spatial light modulator). The phase delay does the modulation through the SLM with patterned quasi-binary phase masks, which comprise two major phase delay values with gradient boundary. Lower panel: The light intensity and SEM images with or without phase masks are compared, showing the improved resolution from the gradient intensity boundary. Reproduced from [238]. CC BY 4.0. (b) The fabrication process of the 'sketch and peel' method (upper panel). The following schematics indicate the selective peeling affected by the initial breakage (middle panel). SEM images show the features of the structures within different steps (lower panel). Reprinted with permission from [245]. Copyright (2016) American Chemical Society.

via self-assembly techniques, and integrating new materials onto plasmonic and dielectric materials to form hybrid nanostructures.

6.1. Accuracy improvement

While the design of devices exhibits robustness, achieving defect-free and accurate fabrication with nanometer precision is crucial to realize a photonic response that closely aligns with theoretical calculations [233–235]. Several reviews have focused on the resolution improvement in the fabrication of integrated circuits [68, 236]. Methods we reviewed here can be categorized according to the optimized process or material, including mask, deposition, substrate, and resist.

Precise design of nanoscale masks facilitates the convergence of beams with high intensity at specified locations. This can be accomplished, for instance, by using plasmonic lithography with more confined intensity [97] or employing phase-shift masks that introduce controlled phase differences to manipulate the focusing of transmitted light [237]. The interference effects are thus improving the location selectivity of exposure. In recent research, a novel approach has been proposed that combines the designed gradient intensity boundaries of phase masks with circular polarization of the wavefront (figure 13(a)). The pattern information from quasi-binary phase masks is transferred into the wavefront and then separated ultrafast laser beam to create periodic ablated nanostructures. This method leads to a significant improvement in resolution by effectively mitigating diffraction and polarization-dependent asymmetric effects during light propagation [238]. Additionally, proximity effect correction is a commonly employed strategy to further enhance resolution in the DLW process [239, 240]. The fundamental concept involves modifying the projection mask to compensate for errors that arise during the projection from the mask to the structure. Similar investigations have been conducted in other direct writing techniques, such as EBL [241] and FIB [242–244].

The deposition process can be optimized with a pre-exposed resist boundary, achieving improved confinement of the as-deposited pattern. Such a method is reported as 'sketch and peel' lithography based on both EBL and FIB (figure 13(b)) [241, 245, 246]. The direct writing method is applied to write the boundary instead of the pattern itself, providing confinement and selectivity for the following peeling steps while reducing the total writing area. Although the same bonding between the deposited metal and substrate exists no matter in and out of the written boundary, the polymer can selectively peel the metal layer because of the random initial breakages, while keeping the metal adhesion inside the boundary. Such selectivity can be modified by boundary design, offering the possibility to peel different materials

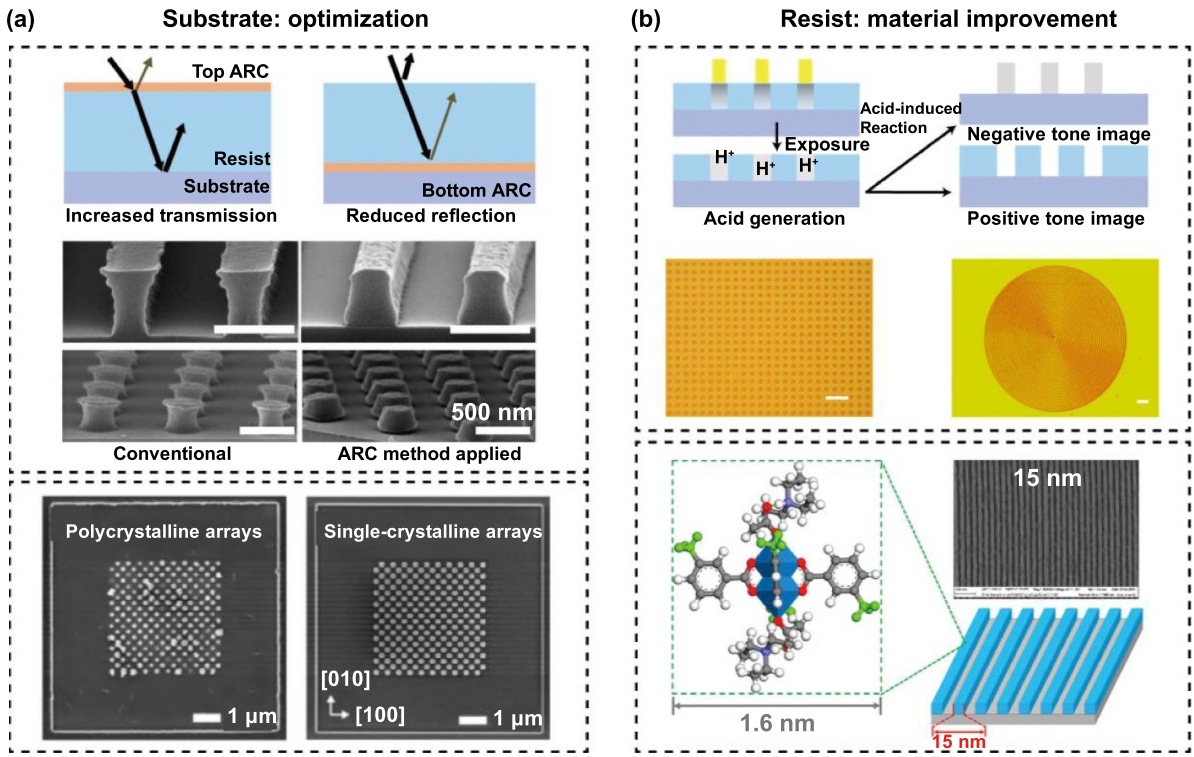

Figure 14. Improvement of fabrication accuracy through material optimization. (a) Upper panel: schematic of anti-reflection coating (ARC) and comparison between fabricated structures with or without ARC applied. The increased transmission through the resist can improve the sensitivity of the resist, while the reduced reflection from the substrate can decrease the reaction exposed by the reflection beam. Reprinted from [252], Copyright © 2011 Elsevier B.V. All rights reserved. Bottom panel: The comparison between the pattern written on muti- and single crystalline Ag nanoarrays produced on SiO_2 substrate. The improvement of the resolution was obtained with FIB at the nanoscale. Reproduced from [257]. CC BY 4.0. (b) Upper panel: schematic of how chemically amplified resist (CAR) works and images of fabricated lattices and rings structures, scale bars are 10 μm. [261] John Wiley & Sons. © 2024 Wiley-VCH GmbH. Bottom panel: Unsymmetric Zn-mTA is exposed to form nano gratings with 15 nm line-and-space dense using extreme ultraviolet lithography. Reprinted with permission from [262]. Copyright (2018) American Chemical Society.

in different layers for heterostructure fabrication [247]. The improved confinement of pattern boundary can uniformly control the narrowest gaps down to 10 nm in large-area arrays. Further, according to the author's claim, hundreds of times of throughput enhancement can be achieved because only the boundary needs to be written. Similarly, masks with extremely sharp patterns are obtained by controlling the falling direction of the resist mask. Sharp structures with a radius of curvature of sub-1 nm are thus fabricated, which were tested in applications such as nanoantennas and surface-enhanced Raman [248–250].

The improvement of materials contributes to the performance of substrate and photoresists in lithography, exerting various effects on the final products. When the wavelength is pushed to extreme ultraviolet for high resolution, the exposure has initially suffered from low source energy and thin resist thickness. Higher sensitivity and absorption efficiency in the resist is thus required [251]. Pre-treatment to a substrate is applied to optimize the response to the lithography beam (figure 14(a)) [252]. The top-coated anti-reflection layer can improve exposure sensitivity by reducing light loss. Moreover, the bottom coated layer can eliminate the standing wave effect from the mismatch of the index on both sides of the resists [253–255]. Another example of an improved substrate is using a single-crystalline substrate to generate accurate and ultrasmooth nanostructures using FIB milling [256, 257]. A continuously expanded material library is also providing possibilities to improve the sensitivity and absorption of resist (figure 14(b)). Chemically amplified resists have improved sensitivity by generating extra catalysts (usually acid) during the exposure process [258–261]. In addition, inorganic and metal-organic frameworks (MOFs) have emerged as a promising alternative to traditional photoresists because of their smaller building units (1–2 nm) than typical polymer photoresists (>3 nm) [251, 262, 263].

6.2. *Shape-define methods*

Direct writing methods are well-suited for generating planar arbitrary patterns, but the preparation of three-dimensional and high aspect ratio units remains challenging. In the case of self-assembly methods, the shape of the assembled units is limited by the self-assembled molecules, and tunable unit shapes are desired. Custom deposition and etching processes, such as reactive ion etching (RIE)/Inductively coupled plasma etching (ICP) undercut etching, tilted angles, pre-deposition films, and annealing, have proven effective in expanding the diversity of unit shape. Moreover, employing suitable post-processing

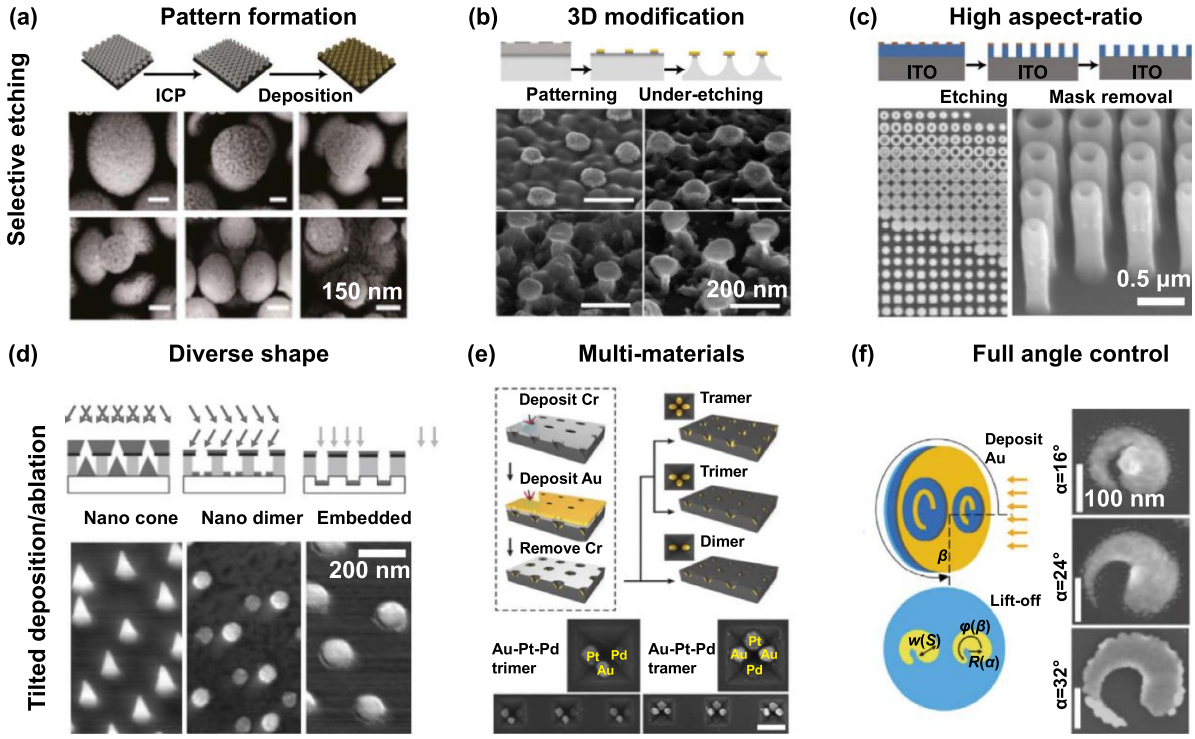

Figure 15. Unit shape definition through selective etching or tilted deposition/ablation. (a) Schematic of fabrication and SEM images of the hierarchical nanoflowers. Different unit shapes are obtained within different etching time. [265] John Wiley & Sons. © 2019 WILEY-VCH Verlag GmbH & Co. KGaA, Weinheim. (b) Schematic of fabrication and SEM images of under-etch nanodisks for index sensing. The mushroom shape is controlled by the etching time. Reproduced from [267]. CC BY 4.0. (c) Fabrication schematic and SEM images of achromatic metalens with different resolutions. A high aspect ratio is achieved by strictly vertical etching. Reproduced from [47]. CC BY 4.0. (d) Fabrication schematics and SEM images of different nanostructure types fabricated by hole mask lithography: cone, disks pair, and embedded disks. [268] John Wiley & Sons. Copyright © 2007 WILEY-VCH Verlag GmbH & Co. KGaA, Weinheim. (e) Schematic and SEM images of hetero-oligomers with tunable materials. A reconstructable mask is applied to locate different materials in one unit together with tilted deposition. Reprinted with permission from [269]. Copyright (2014) American Chemical Society. (f) Non-periodic nanohooks by custom rotation during the metal deposition through a hole mask. Adapted from [270], Copyright © 2019, Tsinghua University Press and Springer-Verlag GmbH Germany, part of Springer.

techniques enables rapid shape definition, reducing the need for repetitive and costly lithography processes to fabricate masks for minor unit shape variations.

6.2.1. Selective etching. Selective ablation or etching techniques are commonly employed to modify the diameter of nanoholes or pillars. Gas or solvent etching methods can selectively modify the components and structures of masks (figure 15(a)) [264, 265]. Further, etching techniques which give orientation selectivity are used as a tool for shaping, enhancing the perpendicularity and smoothness of the sidewalls of the nano unit [266]. Etching processes without clear orientation are used to create mushroom-shaped nanostructures with different selectivity to different layers (figure 15(b)). Such nanostructures effectively increase the bioactive surface area in the unit, thus modifying the optical resonance mode and enhancing its performance in biosensor devices [267]. Moreover, mask-based vertical etching techniques are well-suited for achieving high aspect-ratio structures. Recently, top-down etching was employed to achieve pillar heights exceeding 1.5 μm in a TiO_2 metasurface with a 40 nm minimal feature of pattern (figure 15(c)) [47].

6.2.2. Tilted deposition and ablation. By controlling the deposition or ablation angle, integrating different shapes and materials into one unit is possible. Tilted deposition through holes in the mask has been used to fabricate arrays of elliptical NPs, nanocones, and alloy NPs as shown in figure 15(d) [268], and tilted ablation can create nanopatterns consisting of spots and slits [108]. For example, nano crescent and rhombohedral arrays have been fabricated with tilted deposition before the lift-off of colloidal particles [271–273]. The polarization selective modes and lasing are thus achieved because of the asymmetric units. By utilizing the tilted deposition with sphere masks, sharp tips of the structure can be easily fabricated without high-resolution lithography, accelerating the lasing buildup process and enhancing stimulated emission. Further, units from binary to tetramers can be created for oligomer sensors by depositing different materials from different sides (figure 15(e)) [269]. Tilted deposition can also introduce asymmetric units for chiral or nonlinear optics requiring symmetry breaking [274]. Further, precise control over deposition angle and rotation can make a nanostructure with 'comma-like' nanohook units for chiral optics [270] (figure 15(f)). Moreover, the utilization of tilted deposition is essential for depositing diverse

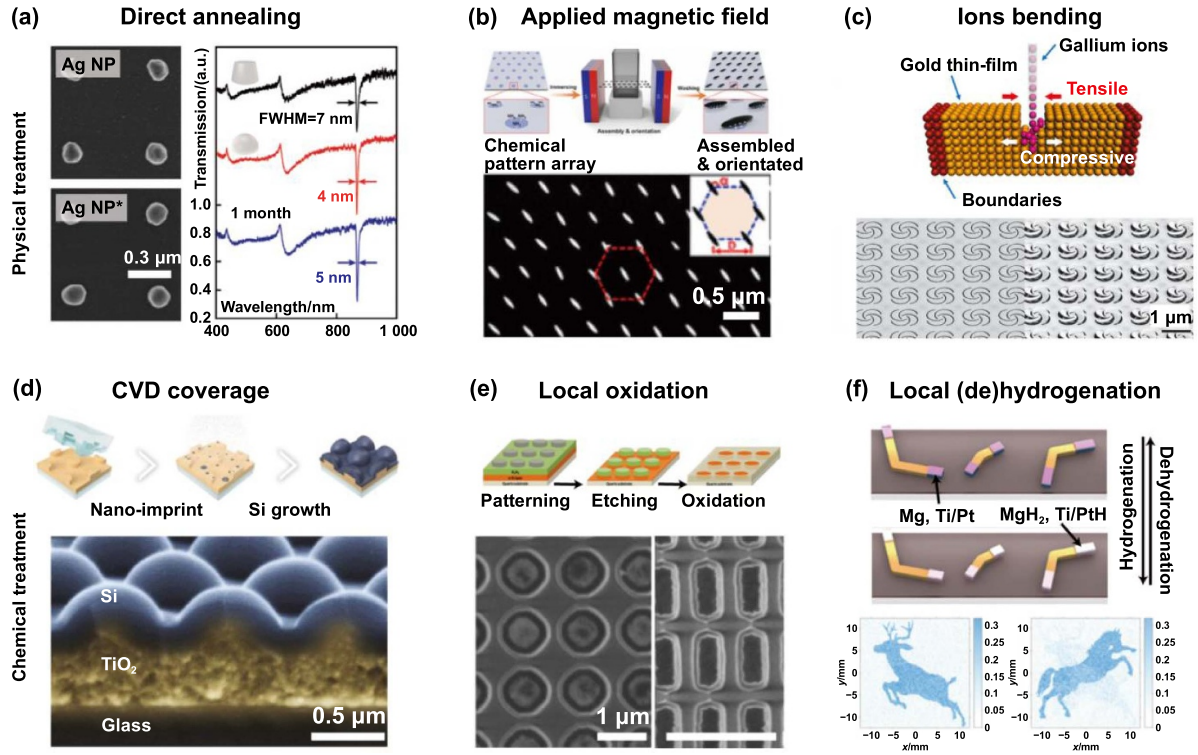

Figure 16. Unit shape definition through physical/chemical post-treatment. (a) Nanoparticles and their collective oscillation before and after annealing. High quality factors can be obtained with relatively stable performance. Reproduced with permission from [276].© 2020. Published under the PNAS license. Author own work. (b) Schematic and SEM images of Fe_3O_4@SiO_2 ellipsoid array with magnetic orientation. Reprinted with permission from [280]. Copyright (2022) American Chemical Society. (c) Upper panel: schematic of residual stress distribution within a free-standing gold nanofilm under FIB irradiation. Reproduced with permission from [285]. Bottom panel: plastic deformation of the silver pattern induced ion beams. [286] John Wiley & Sons. © 2023 Wiley-VCH GmbH. (d) Fabrication schematic and SEM cross-section of the Si-covered TiO_2 arrays. Reproduced from [287]. CC BY 4.0. (e) The fabrication process of ring-disks nanopattern from etching and selective oxidation. SEM images with bright local oxidation edge are shown below. Reprinted with permission from [288]. Copyright (2017) American Chemical Society. (f) Schematic of hydrogenation/dehydrogenation process to the nanostructure results in a modified amplitude and phase of the scattered field. The reconstruction of dynamic images of the complex amplitude profile of the realistic arrays. Reproduced from [289]. CC BY 4.0.

materials onto intricate 3D structures, thereby paving the way for expanded applications in multi-material nanostructure lattices [275].

6.2.3. Post-fabrication treatments. A wide range of post-treatment is developed to tune the structural parameters and optical properties of fabricated nanostructures. For example, annealing is introduced to generate single-crystal of metal NPs with dewetting and shape deformation at high temperatures to optimize their optical performances (figure 16(a)) [276, 277]. Selective electrostatic modification of NPs allows the formation of dimeric nanostructures. In this way, the capillary force and laser exposure are proven to be able to guide the orientation and patterning during the assembling of particles with opposite charges [278, 279]. Another approach involves the use of magnetic interactions to precisely modify magnetic nano ellipsoids across a large area (figure 16(b)), facilitating the formation of oriented arrays. Such ability to control the particle orientation is particularly valuable for chiral and anisotropic studies [280]. In recent work, the swift heavy ions are applied to create tracks in parallel alignment for subsequent wet etching. A randomly distributed array of nano-pores pairs with tip-to-tip configuration can be obtained at the position of the tracks, and a highly localized field is excited around the tips for enhanced SERS detection [281]. Moreover, ion irradiation in FIB induces stress in flat nanostructures to bend or fold them into nano-kirigami leading to flexible programming of 3D nano metasurface (figure 16(c)) [35, 282–286].

Chemical reactions offer a means to adjust the surface of the substrate or nano-unit. In the fabrication of all-dielectric nanostructure lattices, one approach involves utilizing chemical vapor deposition to grow silicon nanosphere arrays on pre-printed TiO_2 arrays (figure 16(d)) [287]. Another effective method is direct local oxidation, which not only modifies the structural size but also alters the local refractive index. This enables rapid adjustment of optical properties without the need for repeated lithography or deposition processes (figure 16(e)) [288, 290]. In addition to the oxidation, a local reconfigurable hydrogenation/dehydrogenation process is employed for reshaping the nanostructure units. This process has demonstrated the dynamic modification of hierarchical reaction kinetics, achieving the reconstructed image from the reshaping of the phase profile allowed by the quantified phase relation (figure 16(f)) [289].

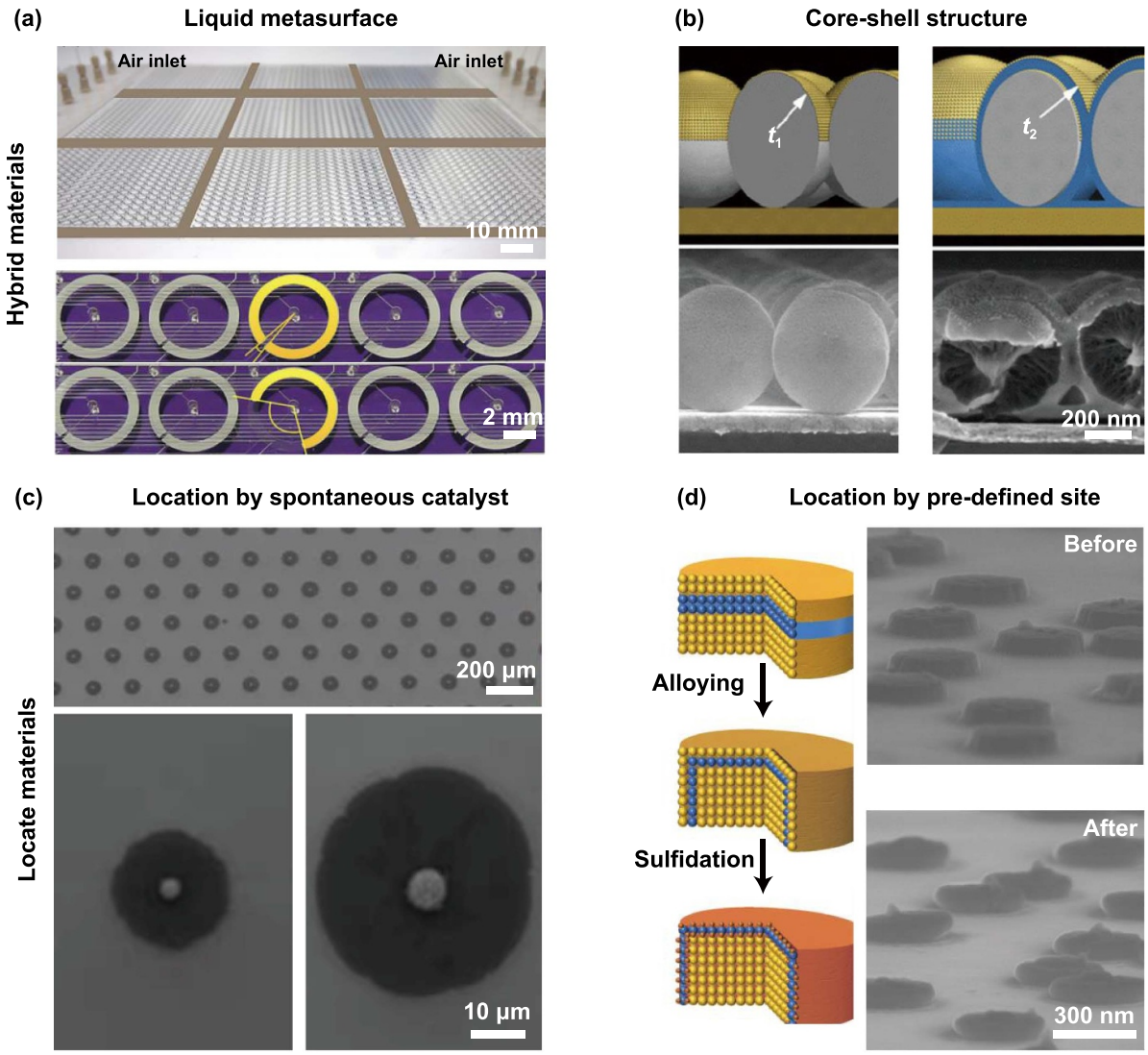

Figure 17. Fabrication of metasurfaces with hybrid structures. (a) An overview and zoom-in view of the liquid plasmonic resonators based on the microfluidic system. Air gaps of 120° and 5° in an opened ring are obtained when the input pressure of hydrochloric vapor changes. Reprinted from [292], with the permission of AIP Publishing. (b) Schematics and corresponding SEM images of metal/spheres/insulator hybrid nanoparticles. Extra metal was deposited to form the half-core-shell structure with absorption enhanced. Reproduced with permission from [303]. © 2019 The Authors. Published by WILEY-VCH Verlag GmbH & Co. KGaA, Weinheim CC BY-NC 4.0 (c) SEM images of the patterned MoS_2 array, which is grown by the catalyst guidance from nanoparticles. Reproduced from [304]. CC BY 4.0. (d) SEM images before and after in-situ growth of TMD on patterned gold disks [305]. Two steps of fabrication including alloying and sulfidation are involved to sulfurize the pre-patterned metallic molybdenum. [305] John Wiley & Sons.© 2020 WILEY-VCH Verlag GmbH & Co. KGaA, Weinheim.

6.3. Hybrid units

The integration of diverse materials enables the creation of the hybrid units in nanostructure lattices such as core-shell, alloy, and layered nanostructures, which can significantly enhance the functionalities of nanostructure lattices. However, achieving large-area integration of different materials poses a significant challenge because of the diverse growth strategies required for different materials and precise position control. In this section, we review preparation strategies and applications of nanostructure lattices with hybrid units.

6.3.1. Hybrid materials. The pursuit of stability in nanostructure lattices has driven the frequent use of noble metals. However, those inert materials are not suitable for some dynamic and responsive applications. Active elements are introduced to the nanostructure lattices for catalytic studies, for example, group X metals (Ni, Pd, and Pt), [291]. Furthermore, liquid metal together with ordinary microfluidic systems has been applied to build reconfigurable nanostructures [292–294]. Mercury (Hg) and toxic-free eutectic gallium-indium (EGaln) have been proven to excite dynamic plasmonic interaction at GHz and THz bands (figure 17(a)). Further studies are expected to be expanded

to optical wavelength with better microfluidic methods. The integration of different materials into lattice units can be achieved through vapor deposition or chemical modification, resulting in heterodimers and core-shell structures. These integrated structures exhibit enhancement in optical plasmonic resonances and catalytic performances [295–298]. For core-shell units, conformal deposition of the dielectric layers with atomic thickness control is demonstrated. Such design usually contributes to the angle insensitivity and extra degree of freedom for optimizations, while more than one Mie resonance can be tuned and surface plasmon can be excited along the edge between dielectric and metal layers [299–301]. As an example, metallic tungsten was deposited on a self-assembled dielectric nano-sphere directly and showed stronger light-matter interaction and broad working wavelength induced by the stereo profile (figure 17(b)) [302]. In addition, the self-assembled polystyrene spheres can be used as the core directly, in which situation the extra lift-off process can be avoided [303].

6.3.2. Selective growth. 2D materials are frequently coated on metallic nanostructures to excite strong light-matter interaction, leading to enhanced absorption, photoluminescence, and nonlinear optics response. The selective catalytic effects of metal particles play a crucial role in achieving controlled thin film growth and fabricating hybrid units consisting of metals and 2D materials, which has been demonstrated in various combinations such selectivity including Cu to graphene [277], Ni to hBN [306], and Pt/Ti to MoS_2/WS_2 (figure 17(c)) [304]. Besides, the site with growth selectivity can also be created by ablated defects or patterned precursors in the unit [277, 305, 307]. Because metallic precursors allow lower reaction temperatures than normal CVD for TMD growth, the shape of metal nanostructures can be maintained to support stronger plasmonic resonances at particle edges (figure 17(d)).

7. Summary and outlook

In summary, we have compiled a comprehensive overview of existing techniques and recent achievements in nanofabrication for nanostructure lattices. The pattern generation methods are introduced from the perspectives of direct writing lithography, self-assembly methods and controllable deposition. Furthermore, nanopattern transfer methods with a specific focus on nanoimprint, are summarized to provide a comparative analysis of different embossing methods. In addition, we focus on the control of unit structures, highlighting the recent progress in precise and complex structures. These advancements in nanofabrication have promoted the research of optical nanostructure lattices toward more predictable properties and practical applications.

Further, we provide several prospects for future studies on the fabrication of nanostructure lattices: (1) opportunities abound in the quest for both low-cost and high-precision fabrication of nanostructures, particularly given the continually expanding material library, including dynamic and flexible materials. (2) Fabrication of multi-layer and 3D structures has been relatively limited, which may be due to poor alignment of patterned masks or the limitation of high-resolution materials for 3D nano-printing. Addressing these gaps can unlock the potential of optical metasurfaces for advanced applications. (3) Phase-change materials have shown great potential for dynamic metasurfaces. The realization of diverse and adaptable dynamic metasurfaces requires efforts for further sophisticated design and precise fabrication. (4) The application of optical nano-structural lattices requires a combination of various techniques to hybridize materials to enhance their diverse optical responses. The compatibility among multiple fabrication techniques still needs to be tested comprehensively in practical applications. With the continuous development of fabrication, we expect further studies of nanostructure lattices will be widely used in both optical devices and functional materials. By utilizing the characteristics and advantages of different fabrication techniques, nanostructure lattices can work as from large-area metalens for space exploration and holography to miniaturization applications such as nanolasers and on-chip optics. Further, the rising of nanostructures integration to new materials can expand their applications to new scenarios, such as medicinal tools and wearable optical devices.

Acknowledgments

This work was supported by the National Natural Science Foundation of China (No. 62275257). The authors also gratefully thank the startup funding from the Shanghai Institute of Microsystem and Information Technology, Chinese Academy of Sciences. VEB thanks the support of the Russian Science Foundation (No. 22-13-00126).

ORCID iD

Shikai Deng https://orcid.org/0000-0002-1895-2072

References

[1] Veselago V G 1968 The electrodynamics of substances with simultaneously negative values of ε and μ *Sov. Phys.—Usp.* **10** 509
[2] Pendry J B, Holden A J, Robbins D J and Stewart W J 1999 Magnetism from conductors and enhanced nonlinear phenomena *IEEE Trans. Microw. Theory Technol.* **47** 2075–84
[3] Shelby R A, Smith D R and Schultz S 2001 Experimental verification of a negative index of refraction *Science* **292** 77–79
[4] Wen X Y and Deng S K 2023 Plasmonic nanostructure lattices for high-performance sensing *Adv. Opt. Mater.* **11** 2300401
[5] Guo C, Yu J Y and Deng S K 2023 Hybrid metasurfaces of plasmonic lattices and 2D materials *Adv. Funct. Mater.* **33** 2302265
[6] Guan J, Park J E, Deng S K, Tan M J H, Hu J T and Odom T W 2022 Light–matter interactions in hybrid material metasurfaces *Chem. Rev.* **122** 15177–203
[7] Ng C, Wesemann L, Panchenko E, Song J C, Davis T J, Roberts A and Gómez D E 2019 Plasmonic near-complete optical absorption and its applications *Adv. Opt. Mater.* **7** 1801660

[8] Li J Z, Li J Y, Zhou S D and Yi F 2021 Metasurface photodetectors *Micromachines* **12** 1584

[9] Wang D Q, Guan J, Hu J T, Bourgeois M R and Odom T W 2019 Manipulating light–matter interactions in plasmonic nanoparticle lattices *Acc. Chem. Res.* **52** 2997–3007

[10] Cheng P J, Huang Z T, Li J H, Chou B T, Chou Y H, Lo W C, Chen K P, Lu T C and Lin T R 2018 High-performance plasmonic nanolasers with a nanotrench defect cavity for sensing applications *ACS Photonics* **5** 2638–44

[11] Li G C, Lei D Y, Qiu M, Jin W, Lan S and Zayats A V 2021 Light-induced symmetry breaking for enhancing second-harmonic generation from an ultrathin plasmonic nanocavity *Nat. Commun.* **12** 4326

[12] Yang J, Li Y Z, Yang Y M, Xie X R, Zhang Z J, Yuan J L, Cai H, Wang D W and Gao F 2024 Realization of all-band-flat photonic lattices *Nat. Commun.* **15** 1484

[13] Patoux A, Agez G, Girard C, Paillard V, Wiecha P R, Lecestre A, Carcenac F, Larrieu G and Arbouet A 2021 Challenges in nanofabrication for efficient optical metasurfaces *Sci. Rep.* **11** 5620

[14] Wang Y H, Mirkin C A and Park S J 2009 Nanofabrication beyond electronics *ACS Nano* **3** 1049–56

[15] Balykin V I, Borisov P A, Letokhov V S, Melentiev P N, Rudnev S N, Cherkun A P, Akimenko A P, Apel P Y and Skuratov V A 2006 Atom “pinhole camera” with nanometer resolution *JETP Lett.* **84** 466–9

[16] Komlenok M S, Tikhodeev S G, Weiss T, Lebedev S P, Komandin G A and Konov V I 2018 All-carbon diamond/graphite metasurface: experiment and modeling *Appl. Phys. Lett.* **113** 041101

[17] Yan C, Li X, Pu M B, Ma X L, Zhang F, Gao P, Guo Y H, Liu K P, Zhang Z J and Luo X G 2019 Generation of polarization-sensitive modulated optical vortices with all-dielectric metasurfaces *ACS Photonics* **6** 628–33

[18] Reyntjens S and Puers R 2001 A review of focused ion beam applications in microsystem technology *J. Micromech. Microeng.* **11** 287–300

[19] Chen Y F 2015 Nanofabrication by electron beam lithography and its applications: a review *Microelectron. Eng.* **135** 57–72

[20] Hu H, Kim H J and Somnath S 2017 Tip-based nanofabrication for scalable manufacturing *Micromachines* **8** 90

[21] Li N X, Xu Z J, Dong Y, Hu T, Zhong Q Z, Fu Y H, Zhu S Y and Singh N 2020 Large-area metasurface on CMOS-compatible fabrication platform: driving flat optics from lab to fab *Nanophotonics* **9** 3071–87

[22] Lu Z X, Zheng J T, Shi J, Zeng B F, Yang Y, Hong W J and Tian Z Q 2021 Application of micro/nanofabrication techniques to on-chip molecular electronics *Small Methods* **5** 2001034

[23] Nayfeh M H 2018 Manipulation and patterning of surfaces (nanolithography) *Fundamentals and Applications of Nano Silicon in Plasmonics and Fullerines: Current and Future Trends* ed M Nayfeh (Elsevier) ch 5, pp 89–137

[24] Ovsianikov A, Malinauskas M, Schlie S, Chichkov B, Gittard S, Narayan R, Löbler M, Sternberg K, Schmitz K P and Haverich A 2011 Three-dimensional laser micro- and nano-structuring of acrylated poly(ethylene glycol) materials and evaluation of their cytoxicity for tissue engineering applications *Acta Biomater.* **7** 967–74

[25] Keller L *et al* 2018 Direct-write of free-form building blocks for artificial magnetic 3D lattices *Sci. Rep.* **8** 6160

[26] Achal R, Rashidi M, Croshaw J, Churchill D, Taucer M, Huff T, Cloutier M, Pitters J and Wolkow R A 2018 Lithography for robust and editable atomic-scale silicon devices and memories *Nat. Commun.* **9** 2778

[27] Kenney M *et al* 2019 Large area metasurface lenses in the NIR region *Proc. SPIE* **11057**

[28] Groves T R 2014 3—Electron beam lithography *Nanolithography: The Art of Fabricating Nanoelectronic and Nanophotonic Devices and Systems* ed M Feldman (Woodhead Publishing) pp 80–115

[29] Shorubalko I, Pillatsch L and Utke I 2016 Direct–write milling and deposition with noble gases *Helium Ion Microscopy* ed G Hlawacek and A Gölzhäuser (Springer International Publishing) pp 355–93

[30] He S X, Tian R, Wu W, Li W D and Wang D Q 2021 Helium-ion-beam nanofabrication: extreme processes and applications *Int. J. Extrem. Manuf.* **3** 012001

[31] Rommel M, Jambreck J D, Ebm C, Platzgummer E, Bauer A J and Frey L 2010 Influence of FIB patterning strategies on the shape of 3D structures: comparison of experiments with simulations *Microelectron. Eng.* **87** 1566–8

[32] Huth M, Porrati F and Dobrovolskiy O V 2017 Focused electron beam induced deposition meets materials science *Microelectron. Eng.* **185–186** 9–28

[33] Winkler R, Schmidt F P, Haselmann U, Fowlkes J D, Lewis B B, Kothleitner G, Rack P D and Plank H 2017 Direct-write 3D nanoprinting of plasmonic structures *ACS Appl. Mater. Interfaces* **9** 8233–40

[34] Lewis B B, Winkler R, Sang X H, Pudasaini P R, Stanford M G, Plank H, Unocic R R, Fowlkes J D and Rack P D 2017 3D Nanoprinting via laser-assisted electron beam induced deposition: growth kinetics, enhanced purity, and electrical resistivity *Beilstein J. Nanotechnol.* **8** 801–12

[35] Pan R H, Li Z C, Liu Z, Zhu W, Zhu L, Li Y L, Chen S Q, Gu C Z and Li J J 2020 Rapid bending origami in Micro/Nanoscale toward a versatile 3D metasurface *Laser Photonics Rev.* **14** 1900179

[36] Cui A J *et al* 2015 Directly patterned substrate-free plasmonic “nanograter” structures with unusual Fano resonances *Light Sci. Appl.* **4** e308

[37] Garcia R, Knoll A W and Riedo E 2014 Advanced scanning probe lithography *Nat. Nanotechnol.* **9** 577–87

[38] Grebenko A K *et al* 2022 Local ultra-densification of single-walled carbon nanotube films: experiment and mesoscopic modeling *Carbon* **196** 979–87

[39] Biswas A, Bayer I S, Biris A S, Wang T, Dervishi E and Faupel F 2012 Advances in top-down and bottom-up surface nanofabrication: techniques, applications & future prospects *Adv. Colloid Interface Sci.* **170** 2–27

[40] Ryu K S, Wang X F, Shaikh K, Bullen D, Goluch E, Zou J, Liu C and Mirkin C A 2004 Integrated microfluidic linking chip for scanning probe nanolithography *Appl. Phys. Lett.* **85** 136–8

[41] Smith J C, Lee K B, Wang Q, Finn M G, Johnson J E, Mrksich M and Mirkin C A 2003 Nanopatterning the chemospecific immobilization of cowpea mosaic virus capsid *Nano Lett.* **3** 883–6

[42] Sun S Q and Leggett G J 2004 Matching the resolution of electron beam lithography by scanning near-field photolithography *Nano Lett.* **4** 1381–4

[43] Maoz R, Frydman E, Cohen S R and Sagiv J 2000 “Constructive nanolithography”: inert monolayers as patternable templates for in-situ nanofabrication of metal-semiconductor-organic surface structures—a generic approach *Adv. Mater.* **12** 725–31

[44] Eigler D M and Schweizer E K 1990 Positioning single atoms with a scanning tunnelling microscope *Nature* **344** 524–6

[45] Crommie M F, Lutz C P and Eigler D M 1993 Confinement of electrons to quantum corrals on a metal surface *Science* **262** 218–20

[46] Rawlings C, Wolf H, Hedrick J L, Coady D J, Duerig U and Knoll A W 2015 Accurate location and manipulation of

nanoscaled objects buried under spin-coated films *ACS Nano* **9** 6188–95
[47] Wang Y J *et al* 2021 High-efficiency broadband achromatic metalens for near-IR biological imaging window *Nat. Commun.* **12** 5560
[48] Su V C, Chu C H, Sun G and Tsai D P 2018 Advances in optical metasurfaces: fabrication and applications *Opt. Express* **26** 13148–82
[49] Yuan D D, Li J, Huang J X, Wang M, Xu S L and Wang X W 2022 Large-scale laser nanopatterning of multiband tunable mid-infrared metasurface absorber *Adv. Opt. Mater.* **10** 2200939
[50] Barton J E and Odom T W 2004 Mass-limited growth in Zeptoliter beakers: a general approach for the synthesis of nanocrystals *Nano Lett.* **4** 1525–8
[51] Yoo J-H *et al* 2019 Scalable light-printing of substrate-engraved free-form metasurfaces *ACS Appl. Mater. Interfaces* **11** 22684–91
[52] Xu Z J, Jiang L, Li X W, Wang A D, Li B H, Huang L L, Lin Z M, Huang J and Lu Y F 2019 Flash ablation of tunable and deep-subwavelength nanogap by using a spatially modulated femtosecond laser pulse for plasmonic application *ACS Appl. Nano Mater.* **2** 4933–41
[53] Maruo S, Nakamura O and Kawata S 1997 Three-dimensional microfabrication with two-photon-absorbed photopolymerization *Opt. Lett.* **22** 132–4
[54] Witzgall G, Vrijen R, Yablonovitch E, Doan V and Schwartz B J 1998 Single-shot two-photon exposure of commercial photoresist for the production of three-dimensional structures *Opt. Lett.* **23** 1745–7
[55] Bentley S J and Boyd R W 2004 Nonlinear optical lithography with ultra-high sub-Rayleigh resolution *Opt. Express* **12** 5735–40
[56] Wu E S, Strickler J H, Harrell W R and Webb W W 1992 Two-photon lithography for microelectronic application *Proc. SPIE* **1674** 776–82
[57] Hong S and Mirkin C A 2000 A nanoplotter with both parallel and serial writing capabilities *Science* **288** 1808–11
[58] Rai-Choudhury P 1997 *Handbook of Microlithography, Micromachining, and Microfabrication. Volume 1, Microlithography* (SPIE Optical Engineering Press)
[59] Semple M, Baladi E and Iyer A K 2019 Optical metasurface based on subwavelength nanoplasmonic metamaterial-lined apertures *IEEE J. Sel. Top. Quantum Electron.* **25** 4700508
[60] Yasuda H, Arai S, Kai J I, Ooae Y, Abe T, Takahashi Y, Hueki S, Maruyama S, Satoru Sago S S and Keiichi Betsui K B 1993 Fast electron beam lithography system with 1024 beams individually controlled by blanking aperture array *Jpn. J. Appl. Phys.* **32** 6012–7
[61] Chang T H P, Mankos M, Lee K Y and Muray L P 2001 Multiple electron-beam lithography *Microelectron. Eng.* **57–58** 117–35
[62] Huo F W, Zheng Z J, Zheng G F, Giam L R, Zhang H and Mirkin C A 2008 Polymer pen lithography *Science* **321** 1658–60
[63] Shim W, Braunschweig A B, Liao X, Chai J N, Lim J K, Zheng G F and Mirkin C A 2011 Hard-tip, soft-spring lithography *Nature* **469** 516–20
[64] Salaita K, Wang Y H, Fragala J, Vega R A, Liu C and Mirkin C A 2006 Massively parallel dip–pen nanolithography with 55 000-pen two-dimensional arrays *Angew. Chem., Int. Ed.* **45** 7220–3
[65] Wang S, Hosford J, Heath W P and Wong L S 2015 Large-area scanning probe nanolithography facilitated by automated alignment of probe arrays *RSC Adv.* **5** 61402–9
[66] Leitis A, Tseng M L, John-Herpin A, Kivshar Y S and Altug H 2021 Wafer-scale functional metasurfaces for mid-infrared photonics and biosensing *Adv. Mater.* **33** 2102232
[67] Lubin S M, Zhou W, Hryn A J, Huntington M D and Odom T W 2012 High-rotational symmetry lattices fabricated by Moiré nanolithography *Nano Lett.* **12** 4948–52
[68] Van Rossum M 2005 Integrated circuits *Encyclopedia of Condensed Matter Physics* ed F Bassani, G L Liedl and P Wyder (Elsevier) pp 394–403
[69] Rice B J 2014 Extreme ultraviolet (EUV) lithography *Nanolithography: The Art of Fabricating Nanoelectronic and Nanophotonic Devices and Systems* ed M Feldman (Woodhead Publishing) ch 2, pp 42–79
[70] Barnola S, Posseme N, Landis S and Darnon M 2017 Patterning challenges in microelectronics *Plasma Etching Processes for CMOS Devices Realization* ed N Posseme (ISTE Press) ch 3, pp 59–94
[71] Dong Y *et al* 2020 Si metasurface half-wave plates demonstrated on a 12-inch CMOS platform *Nanophotonics* **9** 149–57
[72] Hu T *et al* 2018 Demonstration of color display metasurfaces via immersion lithography on a 12-inch silicon wafer *Opt. Express* **26** 19548–54
[73] Park J-S *et al* 2024 All-glass 100 mm diameter visible metalens for imaging the cosmos *ACS Nano* **18** 3187–98
[74] Kim J *et al* 2023 Scalable manufacturing of high-index atomic layer–polymer hybrid metasurfaces for metaphotonics in the visible *Nat. Mater.* **22** 474–81
[75] Park J S, Zhang S Y, She A L, Chen W T, Lin P, Yousef K M A, Cheng J X and Capasso F 2019 All-glass, large metalens at visible wavelength using deep-ultraviolet projection lithography *Nano Lett.* **19** 8673–82
[76] Malinauskas M, Žukauskas A, Hasegawa S, Hayasaki Y, Mizeikis V, Buividas R and Juodkazis S 2016 Ultrafast laser processing of materials: from science to industry *Light Sci. Appl.* **5** e16133
[77] Harinarayana V and Shin Y C 2021 Two-photon lithography for three-dimensional fabrication in micro/nanoscale regime: a comprehensive review *Opt. Laser Technol.* **142** 107180
[78] Ruiz de Galarreta C, Casquero N, Humphreys E, Bertolotti J, Solis J, Wright C D and Siegel J 2022 Single-step fabrication of high-performance extraordinary transmission plasmonic metasurfaces employing ultrafast lasers *ACS Appl. Mater. Interfaces* **14** 3446–54
[79] Trautmann A, Roth G L, Nujiqi B, Walther T and Hellmann R 2019 Towards a versatile point-of-care system combining femtosecond laser generated microfluidic channels and direct laser written microneedle arrays *Microsyst. Nanoeng.* **5** 6
[80] Yang B, Fang X E and Kong J L 2020 Engineered microneedles for interstitial fluid cell-free DNA capture and sensing using iontophoretic dual-extraction wearable patch *Adv. Funct. Mater.* **30** 2000591
[81] Liu Y J, Lee Y H, Lee M R, Yang Y J and Ling X Y 2017 Flexible three-dimensional anticounterfeiting plasmonic security labels: utilizing *Z*-axis-dependent SERS readouts to encode multilayered molecular information *ACS Photonics* **4** 2529–36
[82] Aderneuer T, Fernández O and Ferrini R 2021 Two-photon grayscale lithography for free-form micro-optical arrays *Opt. Express* **29** 39511–20
[83] Li F, Liu S F, Liu W, Hou Z W, Jiang J X, Fu Z, Wang S, Si Y L, Lu S Y and Zhou H W 2023 3D printing of inorganic nanomaterials by photochemically bonding colloidal nanocrystals *Science* **381** 1468–74

[84] Wang H, Liu Y J, Ruan Q F, Liu H L, Ng R J H, Tan Y S, Wang H T, Li Y, Qiu C W and Yang J K W 2019 Off-axis holography with uniform illumination via 3D printed diffractive optical elements *Adv. Opt. Mater.* **7** 1900068

[85] Wang H, Wang H T, Zhang W and Yang J K W 2020 Toward near-perfect diffractive optical elements *via* nanoscale 3D printing *ACS Nano* **14** 10452–61

[86] Ouyang W Q, Xu X Y, Lu W P, Zhao N, Han F and Chen S C 2023 Ultrafast 3D nanofabrication via digital holography *Nat. Commun.* **14** 1716

[87] Wang L, Gong W, Cao X W, Yu Y H, Juodkazis S and Chen Q D 2023 Holographic laser fabrication of 3D artificial compound μ-eyes *Light Adv. Manuf.* **4** 26

[88] Pan L *et al* 2011 Maskless plasmonic lithography at 22 nm resolution *Sci. Rep.* **1** 175

[89] Huang J X, Xu K, Hu J, Yuan D D, Li J, Qiao J Y and Xu S L 2022 Self-aligned plasmonic lithography for maskless fabrication of large-area long-range ordered 2D nanostructures *Nano Lett.* **22** 6223–8

[90] Mojarad N, Gobrecht J and Ekinci Y 2015 Interference lithography at EUV and soft x-ray wavelengths: principles, methods, and applications *Microelectron. Eng.* **143** 55–63

[91] Wang L, Terhalle B, Guzenko V A, Farhan A, Hojeij M and Ekinci Y 2012 Generation of high-resolution Kagome lattice structures using extreme ultraviolet interference lithography *Appl. Phys. Lett.* **101** 093104

[92] Hong F and Blaikie R 2019 Plasmonic lithography: recent progress *Adv. Opt. Mater.* **7** 1801653

[93] Ueno K, Juodkazis S, Shibuya T, Yokota Y, Mizeikis V, Sasaki K and Misawa H 2008 Nanoparticle Plasmon-assisted two-photon polymerization induced by incoherent excitation source *J. Am. Chem. Soc.* **130** 6928–9

[94] Ueno K, Takabatake S, Onishi K, Itoh H, Nishijima Y and Misawa H 2011 Homogeneous nano-patterning using plasmon-assisted photolithography *Appl. Phys. Lett.* **99** 011107

[95] Campbell M, Sharp D N, Harrison M T, Denning R G and Turberfield A J 2000 Fabrication of photonic crystals for the visible spectrum by holographic lithography *Nature* **404** 53–56

[96] Xue G P, Zhai Q H, Lu H O, Zhou Q, Ni K, Lin L Y, Wang X H and Li X H 2021 Polarized holographic lithography system for high-uniformity microscale patterning with periodic tunability *Microsyst. Nanoeng.* **7** 31

[97] Kamali S M, Arbabi E, Kwon H and Faraon A 2019 Metasurface-generated complex 3-dimensional optical fields for interference lithography *Proc. Natl Acad. Sci. USA* **116** 21379–84

[98] Jang J H, Ullal C K, Maldovan M, Gorishnyy T, Kooi S, Koh C and Thomas E 2007 3D micro- and nanostructures via interference lithography *Adv. Funct. Mater.* **17** 3027–41

[99] Lu C and Lipson R H 2010 Interference lithography: a powerful tool for fabricating periodic structures *Laser Photonics Rev.* **4** 568–80

[100] Stankevičius E, Gedvilas M, Voisiat B, Malinauskas M and Račiukaitis G 2013 Fabrication of periodic micro-structures by holographic lithography *Lith. J. Phys.* **53** 227–37

[101] Bagal A *et al* 2017 Large-area nanolattice film with enhanced modulus, hardness, and energy dissipation *Sci. Rep.* **7** 9145

[102] Bae G, Jang D and Jeon S 2021 Scalable fabrication of high-performance thin-shell oxide nanoarchitected materials via proximity-field nanopatterning *ACS Nano* **15** 3960–70

[103] Kagias M, Lee S, Friedman A C, Zheng T Z, Veysset D, Faraon A and Greer J R 2023 Metasurface-enabled holographic lithography for impact-absorbing nanoarchitected sheets *Adv. Mater.* **35** 2209153

[104] Gan Z F *et al* 2022 Spatial modulation of nanopattern dimensions by combining interference lithography and grayscale-patterned secondary exposure *Light Sci. Appl.* **11** 89

[105] Ariga K, Hill J P and Ji Q M 2007 Layer-by-layer assembly as a versatile bottom-up nanofabrication technique for exploratory research and realistic application *Phys. Chem. Chem. Phys.* **9** 2319–40

[106] Cheng Q H, Fang H T, Cao R, Ma Z Y, Wang S, Xie R G, Xia H B and Wang D Y 2022 Interfacial self-assembly of nanoparticles into macroscopic, monolayered films *Supramol. Mater.* **1** 100021

[107] Cao T, Liu K, Lu L, Chui H C and Simpson R E 2019 Large-area broadband near-perfect absorption from a thin chalcogenide film coupled to gold nanoparticles *ACS Appl. Mater. Interfaces* **11** 5176–82

[108] Qu T, Liu F, Lin Y C and Huang Y D 2019 Large-area fabrication of metasurface on microspheres based on colloidal assembly and femtosecond ablation *Proc. SPIE* **10928**

[109] Borah R, Ag K R, Minja A C and Verbruggen S W 2023 A review on self-assembly of colloidal nanoparticles into clusters, patterns, and films: emerging synthesis techniques and applications *Small Methods* **7** 2201536

[110] Zhou S *et al* 2022 Chiral assemblies of pinwheel superlattices on substrates *Nature* **612** 259–65

[111] Vogel N, Goerres S, Landfester K and Weiss C K 2011 A convenient method to produce close- and non-close-packed monolayers using direct assembly at the air–water interface and subsequent plasma-induced size reduction *Macromol. Chem. Phys.* **212** 1719–34

[112] Haynes C L and Van Duyne R P 2001 Nanosphere lithography: a versatile nanofabrication tool for studies of size-dependent nanoparticle optics *J. Phys. Chem.* B **105** 5599–611

[113] Gómez-Graña S *et al* 2013 Au@Ag nanoparticles: halides stabilize {100} facets *J. Phys. Chem. Lett.* **4** 2209–16

[114] Alvarez L, Fernandez-Rodriguez M A, Alegria A, Arrese-Igor S, Zhao K, Kröger M and Isa L 2021 Reconfigurable artificial microswimmers with internal feedback *Nat. Commun.* **12** 4762

[115] Qian F, Pascall A J, Bora M, Han T Y J, Guo S R, Ly S S, Worsley M A, Kuntz J D and Olson T Y 2015 On-demand and location selective particle assembly via electrophoretic deposition for fabricating structures with particle-to-particle precision *Langmuir* **31** 3563–8

[116] Zhang G Q, Lan C W, Bian H L, Gao R and Zhou J 2017 Flexible, all-dielectric metasurface fabricated via nanosphere lithography and its applications in sensing *Opt. Express* **25** 22038–45

[117] Ma C R, Zhou F R, Huang P F, Li M, Zhao F, Liu Y, Du C, Li X P, Guan B O and Chen K 2022 Mass fabrication of WS_2 nanodisks and their scattering properties *Adv. Mater. Technol.* **7** 2200432

[118] Ponomareva E, Volk K, Mulvaney P and Karg M 2020 Surface lattice resonances in self-assembled gold nanoparticle arrays: impact of lattice period, structural disorder, and refractive index on resonance quality *Langmuir* **36** 13601–12

[119] Li R R, Mao H Y, Zhu M H, Yang Y D, Xiong J J and Wang W B 2019 Facile preparation of broadband absorbers based on patternable candle soot for applications of optical sensors *Sens. Actuators* A **285** 111–7

[120] Yildirim D U, Ghobadi A, Soydan M C, Atesal O, Toprak A, Caliskan M D and Ozbay E 2019 Disordered and densely packed ITO nanorods as an excellent lithography-free optical solar reflector metasurface *ACS Photonics* **6** 1812–22
[121] Vinnacombe-Willson G A, Conti Y, Jonas S J, Weiss P S, Mihi A and Scarabelli L 2022 Surface lattice Plasmon resonances by direct in situ substrate growth of gold nanoparticles in ordered arrays *Adv. Mater.* **34** 2205330
[122] Scarabelli L, Vila-Liarte D, Mihi A and Liz-Marzán L M 2021 Templated colloidal self-assembly for lattice Plasmon engineering *Acc. Mater. Res.* **2** 816–27
[123] Flauraud V, Mastrangeli M, Bernasconi G D, Butet J, Alexander D T L, Shahrabi E, Martin O J F and Brugger J 2017 Nanoscale topographical control of capillary assembly of nanoparticles *Nat. Nanotechnol.* **12** 73–80
[124] Zhang H Y *et al* 2021 Direct assembly of vertically oriented, gold nanorod arrays *Adv. Funct. Mater.* **31** 2006753
[125] Lee Y H, Lay C L, Shi W X, Lee H K, Yang Y J, Li S Z and Ling X Y 2018 Creating two self-assembly micro-environments to achieve supercrystals with dual structures using polyhedral nanoparticles *Nat. Commun.* **9** 2769
[126] Lee Y H, Shi W X, Yang Y J, Kao Y C, Lee H K, Chu R R, Pang Y L, Lay C L, Li S Z and Ling X Y 2020 Modulating orientational order to organize polyhedral nanoparticles into plastic crystals and uniform metacrystals *Angew. Chem., Int. Ed.* **59** 21183–9
[127] Bates C M, Maher M J, Janes D W, Ellison C J and Willson C G 2014 Block copolymer lithography *Macromolecules* **47** 2–12
[128] Welander A M, Kang H M, Stuen K O, Solak H H, Müller M, de Pablo J J and Nealey P F 2008 Rapid directed assembly of block copolymer films at elevated temperatures *Macromolecules* **41** 2759–61
[129] Sinturel C, Vayer M, Morris M and Hillmyer M A 2013 Solvent vapor annealing of block polymer thin films *Macromolecules* **46** 5399–415
[130] Ryu D Y, Shin K, Drockenmuller E, Hawker C J and Russell T P 2005 A generalized approach to the modification of solid surfaces *Science* **308** 236–9
[131] Bang J, Bae J, Löwenhielm P, Spiessberger C, Given-beck S A, Russell T P and Hawker C 2007 Facile routes to patterned surface neutralization layers for block copolymer lithography *Adv. Mater.* **19** 4552–7
[132] Jung H, Leibfarth F A, Woo S, Lee S, Kang M, Moon B, Hawker C J and Bang J 2013 Efficient surface neutralization and enhanced substrate adhesion through ketene mediated crosslinking and functionalization *Adv. Funct. Mater.* **23** 1597–602
[133] Bita I, Yang J K W, Jung Y S, Ross C A, Thomas E L and Berggren K K 2008 Graphoepitaxy of self-assembled block copolymers on two-dimensional periodic patterned templates *Science* **321** 939–43
[134] Jung Y S, Chang J B, Verploegen E, Berggren K K and Ross C A 2010 A path to ultranarrow patterns using self-assembled lithography *Nano Lett.* **10** 1000–5
[135] Delgadillo P A R, Gronheid R, Thode C J, Wu H P, Cao Y, Neisser M O, Somervell M, Nafus K and Nealey P F 2012 Implementation of a chemo-epitaxy flow for directed self-assembly on 300-mm wafer processing equipment *Proc. SPIE* **11** 031302
[136] Suh H S, Kim D H, Moni P, Xiong S S, Ocola L E, Zaluzec N J, Gleason K K and Nealey P F 2017 Sub-10-nm patterning via directed self-assembly of block copolymer films with a vapour-phase deposited topcoat *Nat. Nanotechnol.* **12** 575–81
[137] Yang J K W, Jung Y S, Chang J B, Mickiewicz R A, Alexander-Katz A, Ross C A and Berggren K K 2010 Complex self-assembled patterns using sparse commensurate templates with locally varying motifs *Nat. Nanotechnol.* **5** 256–60
[138] Kulkarni A A and Doerk G S 2022 Hierarchical, self-assembled metasurfaces via exposure-controlled reflow of block copolymer-derived nanopatterns *ACS Appl. Mater. Interfaces* **14** 27466–75
[139] Liu W Y, Zhong H, Wang R S and Seeman N C 2011 Crystalline two-dimensional DNA-origami arrays *Angew. Chem., Int. Ed.* **50** 264–7
[140] Lin Q-Y *et al* 2018 Building superlattices from individual nanoparticles via template-confined DNA-mediated assembly *Science* **359** 669–72
[141] Rothemund P W K 2006 Folding DNA to create nanoscale shapes and patterns *Nature* **440** 297–302
[142] Han D R, Pal S, Nangreave J, Deng Z T, Liu Y and Yan H 2011 DNA origami with complex curvatures in three-dimensional space *Science* **332** 342–6
[143] Wang Y F, Wang Y, Breed D R, Manoharan V N, Feng L, Hollingsworth A D, Weck M and Pine D J 2012 Colloids with valence and specific directional bonding *Nature* **491** 51–55
[144] Liu W Y, Tagawa M, Xin H L, Wang T, Emamy H, Li H L, Yager K G, Starr F W, Tkachenko A V and Gang O 2016 Diamond family of nanoparticle superlattices *Science* **351** 582–6
[145] O'Brien M N, Lin H X, Girard M, Olvera de la Cruz M and Mirkin C A 2016 Programming colloidal crystal habit with anisotropic nanoparticle building blocks and DNA bonds *J. Am. Chem. Soc.* **138** 14562–5
[146] Vial S, Nykypanchuk D, Yager K G, Tkachenko A V and Gang O 2013 Linear mesostructures in DNA–nanorod self-assembly *ACS Nano* **7** 5437–45
[147] Xiong H M, van der Lelie D and Gang O 2009 Phase behavior of nanoparticles assembled by DNA linkers *Phys. Rev. Lett.* **102** 015504
[148] Nykypanchuk D, Maye M M, van der Lelie D and Gang O 2008 DNA-guided crystallization of colloidal nanoparticles *Nature* **451** 549–52
[149] Macfarlane R J, Lee B, Jones M R, Harris N, Schatz G C and Mirkin C A 2011 Nanoparticle superlattice engineering with DNA *Science* **334** 204–8
[150] Zhao Y, Dai X P, Wang F, Zhang X L, Fan C H and Liu X G 2019 Nanofabrication based on DNA nanotechnology *Nano Today* **26** 123–48
[151] Kershner R J *et al* 2009 Placement and orientation of individual DNA shapes on lithographically patterned surfaces *Nat. Nanotechnol.* **4** 557–61
[152] Myers B D, Palacios E, Myers D I, Butun S, Aydin K and Dravid V P 2019 Stimuli-responsive DNA-linked nanoparticle arrays as programmable surfaces *Nano Lett.* **19** 4535–42
[153] Jung W *et al* 2021 Three-dimensional nanoprinting via charged aerosol jets *Nature* **592** 54–59
[154] Shin J, Jung Y H, Pikhitsa P V, Hur C, Cho W, Jung W and Choi M 2022 Three-dimensional nanoprinting with charged aerosol focusing via an electrified mask *Addit. Manuf.* **60** 103206
[155] Jung W, Pikhitsa P V, Jung Y H, Shin J, Han M and Choi M 2021 3D nanoprinting with charged aerosol particles—an overview *Acc. Mater. Res.* **2** 1117–28
[156] Mao P, Liu C X, Li X Y, Liu M X, Chen Q, Han M, Maier S A, Sargent E H and Zhang S 2021 Single-step-fabricated disordered metasurfaces for enhanced light extraction from LEDs *Light Sci. Appl.* **10** 180
[157] Liu S R, Ai J G, Zhang Y Q and Feng J C 2024 Programmable and parallel 3D nanoprinting using configured electric fields *Adv. Funct. Mater.* **34** 2308734

[158] Liu B Y, Liu S R, Devaraj V, Yin Y X, Zhang Y Q, Ai J G, Han Y C and Feng J C 2023 Metal 3D nanoprinting with coupled fields *Nat. Commun.* **14** 4920
[159] Vazquez-Mena O, Villanueva G, Savu V, Sidler K, van den Boogaart M A F and Brugger J 2008 Metallic nanowires by full wafer stencil lithography *Nano Lett.* **8** 3675–82
[160] Su P *et al* 2021 Large-area optical metasurface fabrication using nanostencil lithography *Opt. Lett.* **46** 2324–7
[161] Du K, Liu Y Y, Wathuthanthri I and Choi C H 2012 Dual applications of free-standing holographic nanopatterns for lift-off and stencil lithography *J. Vac. Sci. Technol.* B **30** 06FF04
[162] Du K, Ding J J, Wathuthanthri I and Choi C H 2017 Selective hierarchical patterning of silicon nanostructures via soft nanostencil lithography *Nanotechnology* **28** 465303
[163] Savu V, van den Boogaart M A F, Brugger J, Arcamone J, Sansa M and Perez-Murano F 2008 Dynamic stencil lithography on full wafer scale *J. Vac. Sci. Technol.* B **26** 2054–8
[164] Huang M, Galarreta B C, Artar A, Adato R, Aksu S and Altug H 2012 Reusable nanostencils for creating multiple biofunctional molecular nanopatterns on polymer substrate *Nano Lett.* **12** 4817–22
[165] Aksu S, Yanik A A, Adato R, Artar A, Huang M and Altug H 2010 High-throughput nanofabrication of infrared plasmonic nanoantenna arrays for vibrational nanospectroscopy *Nano Lett.* **10** 2511–8
[166] Sopha H, Samoril T, Palesch E, Hromadko L, Zazpe R, Skoda D, Urbanek M, Ng S, Prikryl J and Macak J M 2017 Ideally hexagonally ordered TiO_2 nanotube arrays *ChemistryOpen* **6** 480–3
[167] So S, Hwang I and Schmuki P 2015 Hierarchical DSSC structures based on "single walled" TiO_2 nanotube arrays reach a back-side illumination solar light conversion efficiency of 8% *Energy Environ. Sci.* **8** 849–54
[168] Albu S P, Ghicov A, Aldabergenova S, Drechsel P, LeClere D, Thompson G E, Macak J M and Schmuki P 2008 Formation of double-walled TiO_2 nanotubes and robust anatase membranes *Adv. Mater.* **20** 4135–9
[169] Thuy U T D, Thuy N T, Tung N T, Janssens E and Liem N Q 2019 Large-area cost-effective lithography-free infrared metasurface absorbers for molecular detection *APL Mater.* **7** 071102
[170] Gulati K, Santos A, Findlay D and Losic D 2015 Optimizing anodization conditions for the growth of Titania nanotubes on curved surfaces *J. Phys. Chem.* C **119** 16033–45
[171] Fu Y and Mo A C 2018 A review on the electrochemically self-organized titania nanotube arrays: synthesis, modifications, and biomedical applications *Nanoscale Res. Lett.* **13** 187
[172] Allred D B, Cheng A C, Sarikaya M, Baneyx F and Schwartz D T 2008 Three-dimensional architecture of inorganic nanoarrays electrodeposited through a surface-layer protein mask *Nano Lett.* **8** 1434–8
[173] Wen L Y, Xu R, Mi Y and Lei Y 2017 Multiple nanostructures based on anodized aluminium oxide templates *Nat. Nanotechnol.* **12** 244–50
[174] Lin Q F, Leung S F, Tsui K H, Hua B and Fan Z Y 2013 Programmable nanoengineering templates for fabrication of three-dimensional nanophotonic structures *Nanoscale Res. Lett.* **8** 268
[175] Mozalev A, Bendova M, Gispert-Guirado F, Pytlicek Z and Llobet E 2016 Metal-substrate-supported tungsten-oxide nanoarrays *via* porous-alumina-assisted anodization: from nanocolumns to nanocapsules and nanotubes *J. Mater. Chem.* A **4** 8219–32
[176] Xia Y N, Yang P D, Sun Y G, Wu Y Y, Mayers B, Gates B D, Yin Y D, Kim F and Yan H Q 2003 One-dimensional nanostructures: synthesis, characterization, and applications *Adv. Mater.* **15** 353–89
[177] Hasan M, Schroers J and Kumar G 2015 Functionalization of metallic glasses through hierarchical patterning *Nano Lett.* **15** 963–8
[178] Liu N J, Xie Y J, Liu G N, Sohn S, Raj A, Han G X, Wu B Z, Cha J J, Liu Z and Schroers J 2020 General nanomolding of ordered phases *Phys. Rev. Lett.* **124** 036102
[179] Lee D *et al* 2018 Polarization-sensitive tunable absorber in visible and near-infrared regimes *Sci. Rep.* **8** 12393
[180] Wan Y H, Krueger N A, Ocier C R, Su P, Braun P V and Cunningham B T 2017 Resonant mode engineering of photonic crystal sensors clad with ultralow refractive index porous silicon dioxide *Adv. Opt. Mater.* **5** 1700605
[181] Lee G Y, Hong J Y, Hwang S, Moon S, Kang H, Jeon S, Kim H, Jeong J H and Lee B 2018 Metasurface eyepiece for augmented reality *Nat. Commun.* **9** 4562
[182] Makarov S V *et al* 2017 Multifold emission enhancement in nanoimprinted hybrid perovskite metasurfaces *ACS Photonics* **4** 728–35
[183] Liu Z, Liu N J and Schroers J 2022 Nanofabrication through molding *Prog. Mater. Sci.* **125** 100891
[184] Ahiboz D, Manley P and Becker C 2020 Adjustable large-area dielectric metasurfaces for near-normal oblique incident excitation *OSA Contin.* **3** 971–81
[185] Chehadi Z, Montanari M, Granchi N, Modaresialam M, Koudia M, Abel M, Putero M, Grosso D, Intonti F and Abbarchi M 2022 Soft nano-imprint lithography of rare-earth-doped light-emitting photonic metasurface *Adv. Opt. Mater.* **10** 2201618
[186] Chou S Y, Krauss P R and Renstrom P J 1995 Imprint of sub-25 nm vias and trenches in polymers *Appl. Phys. Lett.* **67** 3114–6
[187] Barbero D R, Saifullah M S M, Hoffmann P, Mathieu H J, Anderson D, Jones G A C, Welland M and Steiner U 2007 High-resolution nanoimprinting with a robust and reusable polymer mold *Adv. Funct. Mater.* **17** 2419–25
[188] Suh K Y, Kim Y S and Lee H H 2001 Capillary force lithography *Adv. Mater.* **13** 1386–9
[189] Liang C C, Lin C H, Cheng T C, Shieh J and Lin H H 2015 Nanoimprinting of flexible polycarbonate sheets with a flexible polymer mold and application to superhydrophobic surfaces *Adv. Mater. Interfaces* **2** 1500030
[190] Khang D Y, Kang H, Kim T I and Lee H H 2004 Low-pressure nanoimprint lithography *Nano Lett.* **4** 633–7
[191] Kumar G, Tang H X and Schroers J 2009 Nanomoulding with amorphous metals *Nature* **457** 868–72
[192] Mukherjee S, Carmo M, Kumar G, Sekol R C, Taylor A D and Schroers J 2012 Palladium nanostructures from multi-component metallic glass *Electrochim. Acta* **74** 145–50
[193] Li R *et al* 2018 Atomic imprinting into metallic glasses *Commun. Phys.* **1** 75
[194] Liu X, Shao Y, Li J F, Chen N and Yao K F 2014 Large-area and uniform amorphous metallic nanowire arrays prepared by die nanoimprinting *J. Alloys Compd.* **605** 7–11
[195] Chu J P, Wijaya H, Wu C W, Tsai T R, Wei C S, Nieh T G and Wadsworth J 2007 Nanoimprint of gratings on a bulk metallic glass *Appl. Phys. Lett.* **90** 034101
[196] Mukherjee S, Sekol R C, Carmo M, Altman E I, Taylor A D and Schroers J 2013 Tunable hierarchical metallic-glass nanostructures *Adv. Funct. Mater.* **23** 2708–13
[197] Liu Z and Schroers J 2015 General nanomoulding with bulk metallic glasses *Nanotechnology* **26** 145301
[198] Kumar G, Desai A and Schroers J 2011 Bulk metallic glass: the smaller the better *Adv. Mater.* **23** 461–76
[199] Gong P, Kou H C, Wang S B, Deng L, Wang X Y and Jin J S 2019 Research on thermoplastic formability and

nanomoulding mechanism of lightweight Ti-based bulk metallic glasses *J. Alloys Compd.* **801** 267–76
[200] Gong P, Wang S B, Liu Z, Chen W, Li N, Wang X Y and Yao K F 2018 Lightweight Ti-based bulk metallic glasses with superior thermoplastic formability *Intermetallics* **98** 54–59
[201] Han G X, Xu L H and Liu Z 2019 Controlled fabrication of hierarchical metal nanostructures *Mater. Lett.* **241** 160–3
[202] Liu Z, Han G X, Sohn S, Liu N J and Schroers J 2019 Nanomolding of crystalline metals: the smaller the easier *Phys. Rev. Lett.* **122** 036101
[203] Liu Z 2019 Investigation of temperature and feature size effects on deformation of metals by superplastic nanomolding *Phys. Rev. Lett.* **122** 016101
[204] Liu Z 2017 One-step fabrication of crystalline metal nanostructures by direct nanoimprinting below melting temperatures *Nat. Commun.* **8** 14910
[205] Ajayan P M and Lijima S 1993 Capillarity-induced filling of carbon nanotubes *Nature* **361** 333–4
[206] Kim M, Lee D, Kim T H, Yang Y, Park H J and Rho J 2019 Observation of enhanced optical spin hall effect in a vertical hyperbolic metamaterial *ACS Photonics* **6** 2530–6
[207] Byun M, Lee D, Kim M, Kim Y, Kim K, Ok J G, Rho J and Lee H 2017 Demonstration of nanoimprinted hyperlens array for high-throughput sub-diffraction imaging *Sci. Rep.* **7** 46314
[208] Lee D *et al* 2018 Realization of wafer-scale hyperlens device for sub-diffractional biomolecular imaging *ACS Photonics* **5** 2549–54
[209] Lee D, Yang Y, Yoon G, Kim M and Rho J 2019 Resolution enhancement of fluorescence microscopy using encoded patterns from all-dielectric metasurfaces *Appl. Phys. Lett.* **115** 101102
[210] Lee D, Kim M, Kim J, Hong H, Badloe T, Kim D S and Rho J 2019 All-dielectric metasurface imaging platform applicable to laser scanning microscopy with enhanced axial resolution and wavelength selection *Opt. Mater. Express* **9** 3248–59
[211] Jeong J W *et al* 2014 High-resolution nanotransfer printing applicable to diverse surfaces via interface-targeted adhesion switching *Nat. Commun.* **5** 5387
[212] Park T W *et al* 2020 Thermally assisted nanotransfer printing with sub–20-nm resolution and 8-inch wafer scalability *Sci. Adv.* **6** eabb6462
[213] Park T W, Jung H, Park J, Ahn Y S, Hong S W, Lee J, Lee J H and Park W I 2021 Topographically designed hybrid nanostructures *via* nanotransfer printing and block copolymer self-assembly *Nanoscale* **13** 11161–8
[214] Zhu J F, Wang Z Y, Lin S W, Jiang S, Liu X Y and Guo S S 2020 Low-cost flexible plasmonic nanobump metasurfaces for label-free sensing of serum tumor marker *Biosens. Bioelectron.* **150** 111905
[215] Zabow G 2022 Reflow transfer for conformal three-dimensional microprinting *Science* **378** 894–8
[216] Allegro I, Bonal V, Mamleyev E R, Villalvilla J M, Quintana J A, Jin Q H, Díaz-García M A and Lemmer U 2023 Distributed feedback lasers by thermal nanoimprint of perovskites using gelatin gratings *ACS Appl. Mater. Interfaces* **15** 8436–45
[217] Wang Z, Hansen C, Ge Q, Maruf S H, Ahn D U, Qi H J and Ding Y F 2011 Programmable, pattern-memorizing polymer surface *Adv. Mater.* **23** 3669–73
[218] Lee S, Lee N, Yeon G, Park J, Choi H, Koo S, Oh D K and Ok J G 2021 Piezo-actuated one-axis vibrational patterning for mold-free continuous fabrication of high-precision period-programmable micro- and nanopatterns *ACS Nano* **15** 3070–8
[219] Oh D K *et al* 2019 Tailored nanopatterning by controlled continuous nanoinscribing with tunable shape, depth, and dimension *ACS Nano* **13** 11194–202
[220] Sayed S and Selvaganapathy P R 2021 Constrained shrinking of nanoimprinted pre-stressed polymer films to achieve programmable, high-resolution, miniaturized nanopatterns *Nanotechnology* **32** 505301
[221] Haisma J, Verheijen M, van den Heuvel K and van den Berg J 1996 Mold-assisted nanolithography: a process for reliable pattern replication *J. Vac. Sci. Technol.* **14** 4124–8
[222] Zhou Y, Shen S, Zhang J, Jin P F and Liu Y H 2015 Fabrication of sub-wavelength antireflective structures using a soft roll-to-plate nanoimprinting lithographic method *Adv. Mater. Res.* **1118** 3–8
[223] Yoon G, Kim I and Rho J 2016 Challenges in fabrication towards realization of practical metamaterials *Microelectron. Eng.* **163** 7–20
[224] Pina-Hernandez C, Guo L J and Fu P F 2010 High-resolution functional epoxysilsesquioxane-based patterning layers for large-area nanoimprinting *ACS Nano* **4** 4776–84
[225] Lee J H *et al* 2017 Rapid and conformal coating of polymer resins by airbrushing for continuous and high-speed roll-to-roll nanopatterning: parametric quality controls and extended applications *Nano Converg.* **4** 11
[226] Wong H C, Grenci G, Wu J, Viasnoff V and Low H Y 2018 Roll-to-roll fabrication of residual-layer-free micro/nanoscale membranes with precise pore architectures and tunable surface textures *Ind. Eng. Chem. Res.* **57** 13759–68
[227] King E, Xia Y N, Zhao X M and Whitesides G M 1997 Solvent-assisted microcontact molding: a convenient method for fabricating three-dimensional structures on surfaces of polymers *Adv. Mater.* **9** 651–4
[228] Hu J T, Wang D Q, Bhowmik D, Liu T T, Deng S K, Knudson M P, Ao X Y and Odom T W 2019 Lattice-resonance metalenses for fully reconfigurable imaging *ACS Nano* **13** 4613–20
[229] Lee M H, Huntington M D, Zhou W, Yang J C and Odom T W 2011 Programmable soft lithography: solvent-assisted nanoscale embossing *Nano Lett.* **11** 311–5
[230] Yang F, Chen Q Y, Wang J J, Chang J J, Dong W H, Cao W, Ye S S, Shi L and Nie Z H 2023 Fabrication of centimeter-scale plasmonic nanoparticle arrays with ultranarrow surface lattice resonances *ACS Nano* **17** 725–34
[231] Lee S H, Rho W Y, Park S J, Kim J, Kwon O S and Jun B H 2018 Multifunctional self-assembled monolayers via microcontact printing and degas-driven flow guided patterning *Sci. Rep.* **8** 16763
[232] Shallcross R C, Chawla G S, Marikkar F S, Tolbert S, Pyun J and Armstrong N R 2009 Efficient CdSe nanocrystal diffraction gratings prepared by microcontact molding *ACS Nano* **3** 3629–37
[233] Jeon J, Hwang J, Bhattarai K, Kim D K, Kim J O, Urbas A, Zhou J F, Ku Z and Lee S J 2019 Robust metamaterial-based antireflection coating for surface plasmon polariton resonance *Opt. Mater. Express* **9** 1290–7
[234] Zhang J H, ElKabbash M, Wei R, Singh S C, Lam B and Guo C L 2019 Plasmonic metasurfaces with 42.3% transmission efficiency in the visible *Light Sci. Appl.* **8** 53
[235] Wang H C, Achouri K and Martin O J F 2022 Robustness analysis of metasurfaces: perfect structures are not always the best *ACS Photonics* **9** 2438–47
[236] Seisyan R P 2011 Nanolithography in microelectronics: a review *Technol. Phys.* **56** 1061–73
[237] Levenson M D, Viswanathan N S and Simpson R A 1982 Improving resolution in photolithography with a

phase-shifting mask *IEEE Trans. Electron Devices* **29** 1828–36
[238] Huang L Y, Xu K, Yuan D D, Hu J, Wang X W and Xu S L 2022 Sub-wavelength patterned pulse laser lithography for efficient fabrication of large-area metasurfaces *Nat. Commun.* **13** 5823
[239] Chen J F, Laidig T L, Wampler K E and Caldwell R F 1997 Practical method for full-chip optical proximity correction *Proc. SPIE* **3051** 790
[240] Kling M *et al* 1998 0.25-μm logic manufacturability using practical 2D optical proximity correction *Proc. SPIE* **3334** 204–14
[241] Chen Y Q, Bi K X, Wang Q J, Zheng M J, Liu Q, Han Y X, Yang J B, Chang S L, Zhang G H and Duan H G 2016 Rapid focused ion beam milling based fabrication of plasmonic nanoparticles and assemblies *via* "sketch and peel" strategy *ACS Nano* **10** 11228–36
[242] Hu H and Bayanheshig 2022 Exploration of a flexible metasurface for strain sensors: a perspective from 2D grating fabrication to spectral characterization *Appl. Sci.* **12** 10007
[243] Chen P, Salemink H W M and Alkemade P F A 2009 Proximity effect in ion-beam-induced deposition of nanopillars *J. Vac. Sci. Technol.* B **27** 1838–43
[244] Flatabø R, Agarwal A, Hobbs R, Greve M M, Holst B and Berggren K K 2018 Exploring proximity effects and large depth of field in helium ion beam lithography: large-area dense patterns and tilted surface exposure *Nanotechnology* **29** 275301
[245] Chen Y Q, Xiang Q, Li Z Q, Wang Y S, Meng Y H and Duan H G 2016 "Sketch and peel" lithography for high-resolution multiscale patterning *Nano Lett.* **16** 3253–9
[246] Zheng M J *et al* 2019 Kirigami-inspired multiscale patterning of metallic structures via predefined nanotrench templates *Microsyst. Nanoeng.* **5** 54
[247] Shu Z W, Chen Y Q, Feng Z Y, Liang H K, Li W Y, Liu Y and Duan H G 2022 Asymmetric nanofractures determined the nonreciprocal peeling for self-aligned heterostructure nanogaps and devices *ACS Appl. Mater. Interfaces* **14** 1718–26
[248] Kim I, Mun J, Baek K M, Kim M, Hao C L, Qiu C W, Jung Y S and Rho J 2020 Cascade domino lithography for extreme photon squeezing *Mater. Today* **39** 89–97
[249] Kim I, Mun J, Hwang W, Yang Y and Rho J 2020 Capillary-force-induced collapse lithography for controlled plasmonic nanogap structures *Microsyst. Nanoeng.* **6** 65
[250] Oh D K, Kim Y, Kim J, Kim I and Rho J 2023 Guided domino lithography for uniform fabrication of single-digit-nanometer scale plasmonic nanoantenna *Nanophotonics* **12** 1435–41
[251] Luo C Y, Xu C C, Lv L, Li H, Huang X X and Liu W 2020 Review of recent advances in inorganic photoresists *RSC Adv.* **10** 8385–95
[252] Park E M, Choi J, Kang B H, Dong K Y, Park Y, Song I S and Ju B K 2011 Investigation of the effects of bottom anti-reflective coating on nanoscale patterns by laser interference lithography *Thin Solid Films* **519** 4220–4
[253] Raut H K, Ganesh V A, Nair A S and Ramakrishna S 2011 Anti-reflective coatings: a critical, in-depth review *Energy Environ. Sci.* **4** 3779–804
[254] Kang W B, Tanaka H, Kimura K, Padmanaban M, Funato S, Kinoshita Y, Kudo T, Nozaki Y and Pawlowski G 1997 Bottom anti-reflective coatings for DUV lithography *J. Photopolym. Sci. Technol.* **10** 471–7
[255] Tanaka T, Hasegawa N, Shiraishi H and Okazaki S 1990 A new photolithography technique with antireflective coating on resist: ARCOR *J. Electrochem. Soc.* **137** 3900–5
[256] Huang J-S *et al* 2010 Atomically flat single-crystalline gold nanostructures for plasmonic nanocircuitry *Nat. Commun.* **1** 150
[257] Mori T, Mori T, Tanaka Y, Suzaki Y and Yamaguchi K 2017 Fabrication of single-crystalline plasmonic nanostructures on transparent and flexible amorphous substrates *Sci. Rep.* **7** 42859
[258] Horibe H, Ishiguro K, Nishiyama T, Kono A, Enomoto K, Yamamoto H, Endo M and Tagawa S 2014 Sensitivity of a chemically amplified three-component resist containing a dissolution inhibitor for extreme ultraviolet lithography *Polym. J.* **46** 234–8
[259] Reichmanis E, Houlihan F M, Nalamasu O and Neenan T X 1994 Chemically amplified resists: chemistry and processes *Adv. Mater. Opt. Electron.* **4** 83–93
[260] Zhang S L *et al* 2023 Chemically amplified molecular glass photoresist regulated by 2-aminoanthracene additive for electron beam lithography and extreme ultraviolet lithography *ACS Omega* **8** 26739–48
[261] Lu X Y, Zhang R S, Yang G W, Li Q, Li B and Wu G P 2024 Aqueous developable and CO_2-sourced chemical amplification photoresist with high performance *Angew. Chem., Int. Ed.* **136** e202401850
[262] Xu H, Sakai K, Kasahara K, Kosma V, Yang K, Herbol H C, Odent J, Clancy P, Giannelis E P and Ober C K 2018 Metal–organic framework-inspired metal-containing clusters for high-resolution patterning *Chem. Mater.* **30** 4124–33
[263] Tu M *et al* 2021 Direct x-ray and electron-beam lithography of halogenated zeolitic imidazolate frameworks *Nat. Mater.* **20** 93–99
[264] Zhu Y, Hou G Z, Wang Q Y, Zhu T, Sun T, Xu J and Chen K J 2022 Silicon-based spectrally selective emitters with good high-temperature stability on stepped metasurfaces *Nanoscale* **14** 10816–22
[265] Jiang T, Goel P, Zhao H, Ma R, Zhu L H, Liu X J and Tang L H 2020 Internal structure tailoring in 3D nanoplasmonic metasurface for surface-enhanced Raman spectroscopy *Part. Part. Syst. Charact.* **37** 1900345
[266] Iyer P P, Pendharkar M, Palmstrøm C J and Schuller J A 2019 III–V heterojunction platform for electrically reconfigurable dielectric metasurfaces *ACS Photonics* **6** 1345–50
[267] Dyrnesli H, Klös G and Sutherland D S 2020 Under-etched plasmonic disks on indium tin oxide for enhanced refractive index sensing on a combined electrochemical and optical platform *Materials* **13** 853
[268] Fredriksson H, Alaverdyan Y, Dmitriev A, Langhammer C, Sutherland D S, Zäch M and Kasemo B 2007 Hole–mask colloidal lithography *Adv. Mater.* **19** 4297–302
[269] Yang A K, Huntington M D, Cardinal M F, Masango S S, Van Duyne R P and Odom T W 2014 Hetero-oligomer nanoparticle arrays for Plasmon-enhanced hydrogen sensing *ACS Nano* **8** 7639–47
[270] Klös G, Andersen A, Miola M, Birkedal H and Sutherland D S 2019 Oxidation controlled lift-off of 3D chiral plasmonic Au nano-hooks *Nano Res.* **12** 1635–42
[271] Bochenkov V E and Sutherland D S 2013 From rings to crescents: a novel fabrication technique uncovers the transition details *Nano Lett.* **13** 1216–20
[272] Knudson M P, Li R, Wang D Q, Wang W J, Schaller R D and Odom T W 2019 Polarization-dependent lasing behavior from low-symmetry nanocavity arrays *ACS Nano* **13** 7435–41
[273] Lin Y H, Wang D Q, Hu J T, Liu J X, Wang W J, Guan J, Schaller R D and Odom T W 2019 Engineering symmetry-breaking nanocrescent arrays for nanolasing *Adv. Funct. Mater.* **29** 1904157

[274] Bochenkov V E and Sutherland D S 2018 Chiral plasmonic nanocrescents: large-area fabrication and optical properties *Opt. Express* **26** 27101–8
[275] Liang Y, Lin H, Koshelev K, Zhang F C, Yang Y Y, Wu J Y, Kivshar Y and Jia B H 2021 Full-stokes polarization perfect absorption with diatomic metasurfaces *Nano Lett.* **21** 1090–5
[276] Deng S K, Li R, Park J E, Guan J, Choo P, Hu J T, Smeets P J M and Odom T W 2020 Ultranarrow plasmon resonances from annealed nanoparticle lattices *Proc. Natl Acad. Sci. USA* **117** 23380–4
[277] Deng S K, Park J E, Kang G, Guan J, Li R, Schatz G C and Odom T W 2022 Interfacial engineering of plasmonic nanoparticle metasurfaces *Proc. Natl Acad. Sci. USA* **119** e2202621119
[278] Ye S S, Zha H, Xia Y F, Dong W H, Yang F, Yi C L, Tao J, Shen X X, Yang D and Nie Z H 2022 Centimeter-scale superlattices of three-dimensionally orientated plasmonic dimers with highly tunable collective properties *ACS Nano* **16** 4609–18
[279] Yang F *et al* 2021 Laser-scanning-guided assembly of Quasi-3D patterned arrays of plasmonic dimers for information encryption *Adv. Mater.* **33** 2100325
[280] Wang Y Z *et al* 2022 Site-selective assembly of centimeter-scale arrays of precisely oriented magnetic nanoellipsoids *ACS Nano* **16** 21208–15
[281] Lyu S, Zhang Y L, Du G H, Di C X, Yao H J, Fan Y L, Duan J L and Lei D Y 2023 Double-sided plasmonic metasurface for simultaneous biomolecular separation and SERS detection *Spectrochim. Acta* A **285** 121801
[282] Rajput N S, Tong Z and Luo X C 2015 Investigation of ion induced bending mechanism for nanostructures *Mater. Res. Express* **2** 015002
[283] Chalapat K, Chekurov N, Jiang H, Li J, Parviz B and Paraoanu G S 2013 Self-organized origami structures via ion-induced plastic strain *Adv. Mater.* **25** 91–95
[284] Liu Z G, Du H F, Li J F, Lu L, Li Z Y and Fang N X 2018 Nano-kirigami with giant optical chirality *Sci. Adv.* **4** eaat4436
[285] Li J F and Liu Z G 2018 Focused-ion-beam-based nano-kirigami: from art to photonics *Nanophotonics* **7** 1637–50
[286] Zhao Y H, Liang Q H, Li S F, Chen Y Y, Liu X, Sun H Z, Wang C, Ji C Y, Li J F and Wang Y 2024 Thermal emission manipulation enabled by nano-kirigami structures *Small* **20** 2305171
[287] Molet P, Gil-Herrera L K, Garcia-Pomar J L, Caselli N, Blanco Á, López C and Mihi A 2020 Large area metasurfaces made with spherical silicon resonators *Nanophotonics* **9** 943–51
[288] Bar-David J, Mazurski N and Levy U 2017 In situ planarization of huygens metasurfaces by nanoscale local oxidation of silicon *ACS Photonics* **4** 2359–66
[289] Li T Y, Wei Q S, Reineke B, Walter F, Wang Y T, Zentgraf T and Huang L L 2019 Reconfigurable metasurface hologram by utilizing addressable dynamic pixels *Opt. Express* **27** 21153–62
[290] Bar-David J, Mazurski N and Levy U 2019 Resonance trimming in dielectric resonant metasurfaces *IEEE J. Sel. Top. Quantum Electron.* **25** 4700705
[291] Connell T U, Bonin G O, Easton C D, Della Gaspera E, Chesman A S R, Davis T J and Gómez D E 2019 Directing energy into a subwavelength nonresonant metasurface across the visible spectrum *ACS Appl. Energy Mater.* **2** 1155–61
[292] Yan L B *et al* 2017 Adaptable metasurface for dynamic anomalous reflection *Appl. Phys. Lett.* **110** 201904
[293] Wang J Q, Liu S C, Guruswamy S and Nahata A 2014 Reconfigurable terahertz metamaterial device with pressure memory *Opt. Express* **22** 4065–74
[294] Hsu L, Ndao A and Kanté B 2019 Broadband and linear polarization metasurface carpet cloak in the visible *Opt. Lett.* **44** 2978–81
[295] Zhang C, Zhao H Q, Zhou L N, Schlather A E, Dong L L, McClain M J, Swearer D F, Nordlander P and Halas N J 2016 Al–Pd nanodisk heterodimers as antenna–reactor photocatalysts *Nano Lett.* **16** 6677–82
[296] Zheng Z K, Tachikawa T and Majima T 2015 Plasmon-enhanced formic acid dehydrogenation using anisotropic Pd–Au nanorods studied at the single-particle level *J. Am. Chem. Soc.* **137** 948–57
[297] Zheng Z K, Tachikawa T and Majima T 2014 Single-particle study of Pt-modified Au nanorods for Plasmon-enhanced hydrogen generation in visible to near-infrared region *J. Am. Chem. Soc.* **136** 6870–3
[298] Della Gaspera E, Bersani M, Mattei G, Nguyen T L, Mulvaney P and Martucci A 2012 Cooperative effect of Au and Pt inside TiO_2 matrix for optical hydrogen detection at room temperature using surface Plasmon spectroscopy *Nanoscale* **4** 5972–9
[299] Sheverdin A and Valagiannopoulos C 2019 Core-shell nanospheres under visible light: optimal absorption, scattering, and cloaking *Phys. Rev.* B **99** 075305
[300] Alù A and Engheta N 2005 Achieving transparency with plasmonic and metamaterial coatings *Phys. Rev.* E **72** 016623
[301] Khlebtsov B, Zharov V, Melnikov A, Tuchin V and Khlebtsov N 2006 Optical amplification of photothermal therapy with gold nanoparticles and nanoclusters *Nanotechnology* **17** 5167–79
[302] Huang Y J *et al* 2022 Wafer-scale self-assembled 2.5D metasurface for efficient near-field and far-field electromagnetic manipulation *Appl. Surf. Sci.* **601** 154244
[303] Yu W W, Lu Y, Chen X R, Xu H, Shao J, Chen X, Sun Y, Hao J M and Dai N 2019 Large-area, broadband, wide-angle plasmonic metasurface absorber for midwavelength infrared atmospheric transparency window *Adv. Opt. Mater.* **7** 1900841
[304] Wang Z D, Huang Q, Chen P, Guo S H, Liu X Q, Liang X L and Wang L 2016 Metal induced growth of transition metal dichalcogenides at controlled locations *Sci. Rep.* **6** 38394
[305] Ma R, Haastrup M J, Wang Z G, Liu Y M, Ye H, Dong M D, Lauritsen J V and Sutherland D S 2020 Direct integration of few-layer MoS_2 at Plasmonic Au nanostructure by substrate-diffusion delivered Mo *Adv. Mater. Interfaces* **7** 1902093
[306] Jeong H, Kim D Y, Kim J, Moon S, Han N M, Lee S H, Okello O F N, Song K, Choi S Y and Kim J K 2019 Wafer-scale and selective-area growth of high-quality hexagonal boron nitride on Ni(111) by metal-organic chemical vapor deposition *Sci. Rep.* **9** 5736
[307] Song I, Park C, Hong M S, Baik J, Shin H J and Choi H C 2014 Patternable large-scale molybdenium disulfide atomic layers grown by gold-assisted chemical vapor deposition *Angew. Chem., Int. Ed.* **53** 1266–9